Cell, Vol. 69, 1227–1236, June 26, 1992, Copyright © 1992 by Cell Press

Rapamycin–FKBP Specifically Blocks Growth-Dependent Activation of and Signaling by the 70 kd S6 Protein Kinases

Jongkyeong Chung,* Calvin J. Kuo,† Gerald R. Crabtree,† and John Blenis*
*Department of Cellular and Molecular Physiology
Harvard Medical School
Boston, Massachusetts 02115
†Howard Hughes Medical Institute
Unit for Molecular and Genetic Medicine, Beckman Center
Stanford University School of Medicine
Stanford, California 94305

Summary

The macrolide rapamycin blocks cell cycle progression in yeast and various animal cells by an unknown mechanism. We demonstrate that rapamycin blocks the phosphorylation and activation of the 70 kd S6 protein kinases (pp70^{S6K}) in a variety of animal cells. The structurally related drug FK506 had no effect on pp70^{S6K} activation but at high concentrations reversed the rapamycin-induced block, confirming the requirement for the rapamycin and FK506 receptor, FKBP. Rapamycin also interfered with signaling by these S6 kinases, blocking serum-stimulated S6 phosphorylation and delaying entry of Swiss 3T3 cells into S phase. Neither rapamycin nor FK506 blocked activation of a distinct family of S6 kinases (RSKs) or the MAP kinases. These studies identify a rapamycin-sensitive signaling pathway, argue for a ubiquitous role for FKBPs in signal transduction, indicate that FK506–FKBP–calcineurin complexes do not interfere with pp70^{S6K} signaling, and show that in fibroblasts pp70^{S6K}, not RSK, is the physiological S6 kinase.

Introduction

Tightly regulated protein phosphorylation signaling cascades promote the transduction of extracellular signals to various intracellular targets that regulate the transcriptional and translational machinery in cells. Two distinct families of growth factor–regulated S6 protein kinases have been identified that function in these signaling processes, the *rsk*-encoded 85–92 kd S6 kinases (Jones et al., 1988; Alcorta et al., 1989; referred to as RSK or pp90^{rsk}) and the 70 kd and 85 kd S6 kinases (Banerjee et al., 1990; Kozma et al., 1990; referred to as pp70^{S6K}). Although both families of S6 kinases are activated rapidly after addition of growth factors to quiescent cells, several studies indicate that RSK and pp70^{S6K} can be regulated by distinct signaling pathways (Chen and Blenis, 1990; Ballou et al., 1991; Blenis et al., 1991; Jurivich et al., 1991). The upstream participants in the signaling pathway leading to the activation of RSK are now being identified. However, little is known about the effectors participating in the regulation of the 70 kd and 85 kd S6 kinases (αII and αI forms, respectively) (Grove et al., 1991) and the physiological role of this signaling pathway.

The RSKs are phosphorylated and activated by the *erk*-encoded MAP kinases. Although MAP kinases are activated by tyrosine and threonine phosphorylation, receptor tyrosine kinases have not been shown to directly phosphorylate and activate them in vitro (for review see Blenis, 1991; Cobb et al., 1991; Sturgill and Wu, 1991). Recent studies demonstrate that c-Ras can mediate signal transduction from receptor tyrosine kinases to the MAP kinases, RSKs, and c-Raf (Wood et al., 1992; Thomas et al., 1992), indicating that the mechanism of activation of the MAP kinases is complex. Downstream, the nuclear and cytoplasmic localization of MAP kinases and RSKs (Chen et al., 1992) and their temporal regulation (Chen et al., 1991; Chung et al., 1991a) are consistent with the possibility that these activated protein kinases can transmit growth-modulatory information in the nucleus and participate in the regulation of immediate-early gene expression. Indeed, several transcription factors have been identified as in vitro targets of these enzymes (Alvarez et al., 1991; Pulverer et al., 1991; Chen et al., 1992). The 70 kd S6 kinases have not been shown to phosphorylate RSK substrates other than the 40S ribosomal protein S6. S6 phosphorylation in cultured cells correlates temporally with the regulation of pp70^{S6K}. Additionally, inhibition of protein synthesis results in the activation of pp70^{S6K} but not pp90^{rsk}, and under these conditions S6 becomes phosphorylated (Blenis et al., 1991). However, RSK may also participate in early G1 phosphorylation of S6 in cultured cells (Sweet et al., 1990) or during Xenopus oocyte maturation (Erikson and Maller, 1989). Understanding the regulation of S6 phosphorylation is important, since there is evidence that S6 phosphorylation participates in the regulation of protein synthesis (Erikson, 1991; Sturgill and Wu, 1991; and references therein). Thus, these distinct S6 kinase families may separately coordinate growth-stimulated changes in transcription and translation.

FK506-binding proteins (FKBPs) are evolutionarily conserved and ubiquitously expressed proteins that should be considered as a potential participant in the signal transduction pathways of many cell systems (for review see Schreiber, 1991). Therefore, its ligands, FK506 and rapamycin, may be useful reagents for delineating signal transduction pathways in many cell types. Rapamycin and FK506 are structurally related macrolides that have been found to inhibit T cell proliferation potently (Schreiber, 1991). Inhibition of T cell growth is mediated by their binding to the cellular receptor FKBP, a cis-trans prolyl isomerase (Siekierka et al., 1989; Harding et al., 1989). Although binding of either drug inhibits FKBP isomerase activity, inhibition of this activity has been dissociated from the ability of these drugs to inhibit T cell activation (Bierer et al., 1990a, 1990b). Indeed, several lines of evidence indicate that these drugs interfere with distinct T cell signal transduction systems (Dumont et al., 1990b; Bierer et al., 1990a). Thus, despite their similarities, it appears that rapamycin and FK506 work by biologically distinct mechanisms. It is also clear that binding to the FKBP is essential

for their biological activities, as the action of one drug can be antagonized by an excess of the other (Bierer et al., 1990a; Dumont et al., 1990a).

A Ca^{2+}/calmodulin-dependent phosphatase, calcineurin, interacts with and is inhibited by the FK506–FKBP complex (Liu et al., 1991). Similar associations are observed with the structurally unrelated but functionally related cyclosporin A–cyclophilin complexes. These complexes also interfere with the nuclear association of a subunit of the T cell transcription factor, NF-AT, which participates in the regulation of early T cell gene expression (Flanagan et al., 1991). Surprisingly, rapamycin–FKBP neither binds to calcineurin nor inhibits NF-AT nuclear association following T cell activation (Liu et al., 1991; Flanagan et al., 1991), indicating that the rapamycin–FKBP complex may utilize a distinct ternary effector protein. The relationship between calcineurin binding and NF-AT nuclear accumulation, and the role of the ubiquitous calcineurin in signal transduction is currently unclear. The mechanism by which rapamycin interferes with cell proliferation is also not known, nor is much known about the biological activity of FKBP (for reviews, see Chang et al., 1991; Morris, 1991; Schreiber, 1991). However, it is worth noting that rapamycin suppresses a wider spectrum of T and B cells than FK506 does (Chang et al., 1991) and irreversibly arrests Saccharomyces cerevisiae proliferation in G1 (Heitman et al., 1991), indicating that the rapamycin-sensitive signaling system is highly conserved.

Based on the information provided above, we supposed that FK506 or rapamycin might affect the RSK or $pp70^{S6K}$ signal transduction systems. We show that rapamycin but not FK506 blocks the activation of the 70 and 85 kd S6 protein kinases. In contrast, rapamycin does not block the activation of the MAP kinases or RSKs. The ability of rapamycin to prevent $pp70^{S6K}$ activation is dependent upon the binding of rapamycin to FKBP. Our results therefore demonstrate that the target(s) of the rapamycin-sensitive signaling pathway participate in the regulation of $pp70^{S6K}$ by a variety of mitogens; that the postulated rapamycin target is ubiquitous; that the FK506 and cyclosporine A target calcineurin does not influence the activities of MAP kinase, RSK, or $pp70^{S6K}$; and that $pp70^{S6K}$, not $pp90^{rsk}$, is the S6 kinase operating in vivo. Finally, the observation that rapamycin delays entry into S phase in fibroblasts and inhibits entry into S phase in T cells is consistent with an important role for the $pp70^{S6K}$ signal transduction system in the regulation of cell proliferation in nonlymphoid cells as well as in lymphoid cells.

Results

Rapamycin Blocks Activation of $pp70^{S6K}$ but Not RSK

Using peptide antibodies derived against the predicted amino terminus (amino acids 20–39) and carboxyl terminus (amino acids 502–525) of $pp70^{S6K}$ (based on Banerjee et al., 1990), we have developed immune complex S6 protein kinase assays that allow us to specifically immunopurify and measure the activity of $pp70^{S6K}$ from cell-free lysates. We have similarly developed specific immune complex assays for two other growth-regulated protein kinases referred to as RSK (Chen and Blenis, 1990) and MAP kinase ($pp44^{mapk/erk1}$) (Wood et al., 1992).

Because of the ubiquitous nature of FKBP, we wished to determine whether FK506 or rapamycin might interfere with mitogen-regulated signaling in fibroblasts. These reagents had little effect on the growth-stimulated activation of the MAP kinase/RSK signal transduction system. Surprisingly, rapamycin but not FK506 dramatically blocked the activation of $pp70^{S6K}$ (Figure 1). In Swiss 3T3 fibroblasts and chicken embryo fibroblasts, $pp70^{S6K}$ has been shown to be activated under a variety of conditions. Rapamycin blocked the stimulation of $pp70^{S6K}$ following activation by: a receptor tyrosine kinase (epidermal growth factor [EGF] receptor), the viral *src* oncogene product (v-*src*), protein kinase C by tumor-promoting phorbol esters, calcium ionophore–induced Ca^{2+} signaling, signal transducing G proteins (bombesin receptor), heat shock (Jurivich et al., 1991), and inhibition of protein synthesis (cycloheximide), as well as by serum growth factors (see Figure 2). Similar results have been observed in HeLa, PC12, and T cells (unpublished data and Figure 9). Thus, signals from very diverse agents in many cell types rapidly converge, leading to the common activation of $pp70^{S6K}$. Rapamycin therefore blocks the signaling or relay process at $pp70^{S6K}$ or at some point membrane proximal to $pp70^{S6K}$.

Half-maximal rapamycin-mediated inhibition of $pp70^{S6K}$ activation by serum growth factors in Swiss 3T3 cells was between 0.04 and 0.4 ng/ml rapamycin (Figure 2A), similar to the rapamycin concentrations used to inhibit T cell proliferation and $pp70^{S6K}$ activity (Figure 9 and Kuo et al., unpublished data). In these experiments rapamycin was added 30 min prior to addition of stimulus as previously described (Flanagan et al., 1991). However, pretreatment was not necessary to block $pp70^{S6K}$ activation, and addition of rapamycin to serum-stimulated cells containing maximally activated $pp70^{S6K}$ resulted in its rapid inactivation with a half-time of approximately 2 min (Figure 2B). The ability of rapamycin to prevent the activation did not require protein synthesis (Figure 1).

Rapamycin completely blocked the activation of $pp70^{S6K}$ throughout early G1 but had no effect on the serum-stimulated activation of the MAP kinases or RSKs. Interestingly, rapamycin had a mildly positive effect on the MAP kinases and RSKs at the earliest time point, with little effect at later stages of the regulation process (Figure 2C).

Rapamycin Blocks $pp70^{S6K}$ Phosphorylation

To determine whether rapamycin directly inhibited $pp70^{S6K}$, we incubated rapamycin and rapamycin–FKBP12 complexes with activated $pp70^{S6K}$ or with inactivated $pp70^{S6K}$ from rapamycin-pretreated cells. No effect on S6 phosphotransferase activity was detected under these conditions (Figure 3). Additional preliminary in vitro studies examining the effects of lysates from rapamycin-treated cells on the phosphorylation or dephosphorylation of $pp70^{S6K}$ were also negative (not shown). $pp70^{S6K}$ is regulated by serine/threonine phosphorylation, presumably by upstream activating kinases. We wished to examine further the possibilities that rapamycin either inhibited the phosphorylated en-

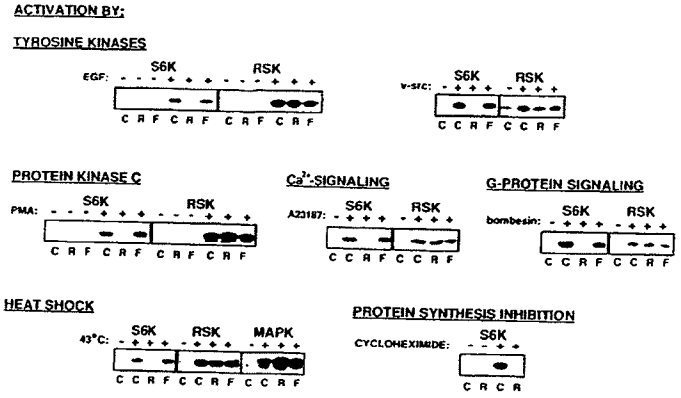

Figure 1. Rapamycin Inhibits pp70^{S6K} Activities Stimulated by a Variety of Conditions

Quiescent (−) Swiss 3T3 cells were stimulated (+) with EGF (25 ng/ml, 10 min), phorbol myristate acetate (100 ng/ml, 10 min), A23187 (25 μM, 30 min), or cycloheximide (100 μM, 30 min), and quiescent (−) bombesin-sensitive 3T3 cells were incubated (+) with bombesin (20 nM, 10 min). Quiescent chicken embryo fibroblasts infected with the temperature-sensitive transformation mutant of Rous sarcoma virus (NY72-4) were stimulated by activation of pp60$^{v\text{-}src}$ following transfer of cultured cells from the nonpermissive temperature (41.5°C, −) to the permissive temperature (35°C, +) for 30 min. For heat shock experiments, quiescent Swiss 3T3 cells grown at 37°C (−) were transferred to 43°C (+) and incubated for 30 min. All cells were pretreated with a vehicle for the drugs (ethanol, 1 μl/ml, marked "C"), rapamycin (20 ng/ml, "R"), or FK506 (20 ng/ml, "F") for a total of 30 min. Cell lysates were prepared after the indicated stimulation time and used for immune complex phosphotransferase assays measuring pp70^{S6K} (S6K), RSK, or MAP kinase (MAPK) activities. We have previously shown that heat shock activates pp70^{S6K} and RSK activities (Jurivich et al., 1991); here we also demonstrate that heat shock activates MAP kinase activity, which is not affected by FK506 or rapamycin. Cycloheximide does not significantly stimulate RSK and MAP kinase activities (Blenis et al., 1991), and thus those assays are not shown in this panel. Phosphorylated S6 (pp70^{S6K} and RSK substrate) and recombinant RSK (MAP kinase substrate) polypeptides were separated by SDS–12% or 7.5% polyacrylamide gel electrophoresis, respectively, and localized by autoradiography.

zyme or blocked its phosphorylation and activation. Serum stimulation of quiescent cells resulted in reduced electrophoretic mobility of both the αI and αII forms of pp70^{S6K} as a result of phosphorylation. Dramatically, pp70^{S6K} (αI and αII) was rapidly dephosphorylated in the presence of rapamycin (Figure 4A), correlating with inactivation of kinase activity (Figure 2B). In addition, immunoblot analysis indicates that the αI form exists at approximately 10- to 20-fold lower levels in the cytosol fraction of Swiss 3T3 fibroblasts than the 70 kd αII form does (Figure 4A), as determined using phosphoimager analysis (Molecular Dynamics, Sunnyvale, CA). To confirm that these mobility shifts are due to the extent of pp70^{S6K} phosphorylation, we tested the ability of potato acid phosphatase to inactivate and dephosphorylate pp70^{S6K} to a form that comigrates with pp70^{S6K} from rapamycin-treated cells (Figure 4B). Notably, the extent of phosphorylation of the αI and αII forms in rapamycin-treated cells based on immunoblot analysis (Figure 4) and biosynthetic labeling (see Figure 6) was less than observed in quiescent cells, consistent with Figures 1 and 2 in which pp70^{S6K} activity in rapamycin-treated cells is lower than in quiescent cells.

Rapamycin could elicit net pp70^{S6K} dephosphorylation either by blocking the activity of an upstream pp70^{S6K}-activating kinase(s) or by stimulating a pp70^{S6K}-specific phosphatase. To examine the latter possibility, we tested the ability of rapamycin to block pp70^{S6K} phosphorylation and activation in the presence of the phosphatase inhibitors, calyculin A and okadaic acid (potent inhibitors of type 1C and 2A protein serine/threonine phosphatases), and vanadate (a potent general inhibitor of protein tyrosine phosphatases). Addition of these phosphatase inhibitors to quiescent cells, alone or in combination, resulted in the phosphorylation and activation of pp70^{S6K} as observed with serum stimulation, and rapamycin blocked these events (Figure 4C and data not shown). RSK activation by calyculin A or vanadate was not affected by rapamycin (Figure 4C), demonstating that the phosphatase inhibitors were active in the presence of rapamycin. Thus, if rapamycin activates a pp70^{S6K}-specific phosphatase, it appears not to be related to phosphatases sensitive to the inhibitors used above. Furthermore, incubation of activated pp70^{S6K} with lysates from untreated or rapamycin-treated cells, in the absence of phosphatase inhibitors, showed no difference in the rate of pp70^{S6K} inactivation (not shown).

FKBP Is Required for the Rapamycin-Induced Block of pp70^{S6K} Phosphorylation and Activation

A consequence of rapamycin and FK506 binding a common receptor, FKBP, is that they are mutually antagonistic when one drug is present at a high molar excess over the other (Bierer et al., 1990a; Dumont et al., 1990a). Accordingly, FK506 reversed the rapamycin block of pp70^{S6K} activation (Figures 5A and 5B) and phosphorylation (Figure 5C) following stimulation of quiescent cells. An FK506:rapamycin ratio of approximately 500:1 was needed for half-maximal reversal of the rapamycin effect, with nearly complete reversal observed at a ratio of 2000:1. These ratios are consistent with a rapamycin–FKBP complex being the active species causing pp70^{S6K} inactivation. This result also demonstrates that FKBPs operate ubiquitously.

Rapamycin Prevents pp70^{S6K} Downstream Signaling

In addition to the inability of rapamycin or FK506 to block MAP kinase or RSK phosphorylation and activation, these immunosuppressants did not affect EGF-stimulated tyrosine phosphorylation, phosphorylation of c-Raf, the serum-stimulated phosphorylation of the transcription fac-

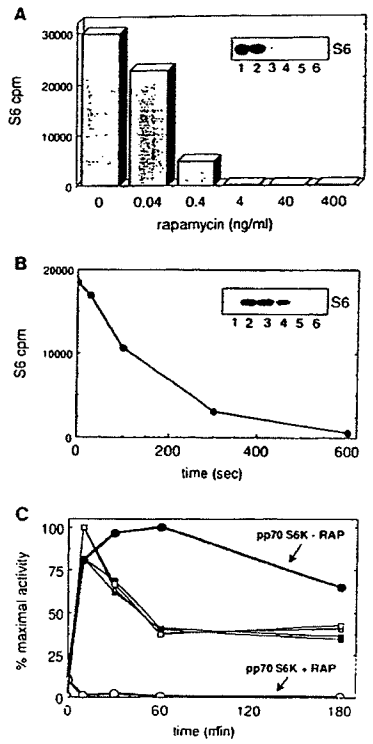

Figure 2. Dose Response and Kinetics of the Inhibition of pp70^{S6K} Phosphotransferase Activity in Swiss 3T3 Cells by Rapamycin

(A) Calf serum (10%) was added to quiescent cells for 10 min following pretreatment with various concentrations of rapamycin for 30 min. pp70^{S6K} activities were measured by the immune complex assay, and incorporation of ^{32}P into S6 was determined after polyacrylamide gel electrophoresis (see inset). Lanes 1–6 in the insert correspond to rapamycin from 0–400 ng/ml as shown in the bar graph. A concentration of 1 ng/ml rapamycin is approximately 1 nM.

(B) Swiss 3T3 fibroblasts containing maximally activated pp70^{S6K} obtained by stimulation of quiescent cells with calf serum (10% [v/v]) were incubated with rapamycin (20 ng/ml) for the final 0, 30, 100, 300, and 600 s of serum stimulation. All cells were lysed after a total of 40 min in the presence of serum and processed for pp70^{S6K} immune complex assays. ^{32}P incorporation into S6 (inset) was determined by scintillation counting. In the insert is shown the incorporation into S6 in quiescent, control cells (lane 1), cells stimulated with serum for 40 min without rapamycin (lane 2), or stimulated cells incubated with rapamycin for 30, 90, 300, and 600 s (lanes 3–6).

(C) Quiescent cells were incubated with 10% calf serum for 0, 10, 30, 60, and 180 min. Cells were pretreated with rapamycin (20 ng/ml, open symbols) or ethanol (1 μl/ml, closed symbols) for 30 min prior to the addition of serum. Cells were lysed, immune complexes formed, and the activities of pp70^{S6K} (open and closed circles), RSK (open and closed triangles), and MAP kinase (open and closed squares) measured as described in Experimental Procedures.

tors such as serum response factor, c-Jun, or Nur77 (not shown and Figure 6), or the overall serum-stimulated phosphorylation of abundant cellular phosphoproteins as examined by SDS–polyacrylamide gel electrophoresis analysis, with the exception of pp70^{S6K} (Figures 4–6) and a single 32 kd phosphoprotein (Figure 7). Since 40S ribo-

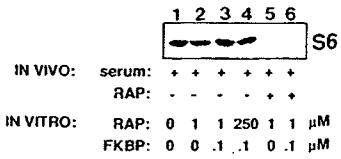

Figure 3. In Vitro Phosphorylation of S6 by Activated or Inactive pp70^{S6K} Is Unaffected by Rapamycin and/or FKBP

pp70^{S6K} activities were purified by immunoprecipitation from quiescent Swiss 3T3 cells stimulated for 10 min with 10% calf serum with or without pretreatment with rapamycin (20 ng/ml). The enzymes in the immune complex were incubated with different concentrations of rapamycin and/or purified FKBP, as indicated in the figure, for 15 min at 30°C in a reaction buffer containing 20 mM HEPES (pH 7.2), 10 mM $MgCl_2$, 100 μg/ml bovine serum albumin, and 30 μM β-mecaptoethanol. [γ-^{32}P]ATP was then added with 40S subunits and S6 phosphotransferase activity measured as described in Experimental Procedures.

somal protein S6 is also ~32 kd, we determined whether phosphorylation of S6 in purified 80S subunits from ^{32}P-labeled cells was blocked by rapamycin. Multiple S6 kinases have been proposed to participate in the physiologi-

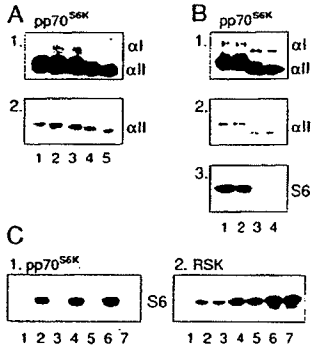

Figure 4. Rapamycin-Induced Dephosphorylation of pp70^{S6K}

(A) Immunopurified pp70^{S6K} polypeptides from cell lysates prepared as described in Figure 2B were used for immunoblotting analysis. pp70^{S6K} was immunoprecipitated from equal amounts of cell lysate protein (250 μg) at each time point. The immunoblot was exposed to X-ray film for 4 hr (panel 2) and 30 hr (panel 1) to show clearly the αI and αII forms, as indicated. Lanes 1, 2, 3, 4, and 5 correspond to incubation of cells containing activated pp70^{S6K} with rapamycin (20 ng/ml) for 0, 30, 100, 300, and 600 s, respectively.

(B) pp70^{S6K} was immunopurified from cell lysates that were stimulated with calf serum for 10 min without (lanes 1, 2, and 3) or with (lane 4) pretreatment of rapamycin (20 ng/ml) for 30 min. Immune-complexed pp70^{S6K} was incubated with heat-inactivated potato acid phosphatase (lane 2), native phosphatase (lane 3), or phosphatase reaction buffer alone (lanes 1 and 4). Phosphatase-treated immune complexes were compared with the untreated controls by immunoblot analysis (panels 1 and 2 showing the αI and αII forms, respectively) and S6 phosphotransferase activity assays (panel 3). Panels 1 and 2 were from the same gel and were exposed to X-ray film for 16 hr and 2 hr, respectively.

(C) Quiescent Swiss 3T3 cells were treated with calyculin A (10 nM, 30 min, lanes 2 and 3) and sodium orthovanadate (500 μM, 30 min, lanes 4 and 5) or with calyculin A and vanadate together (lanes 6 and 7), without (lanes 2, 4, and 6), or with (lanes 3, 5, and 7) pretreatment of rapamycin (20 ng/ml) for 30 min. pp70^{S6K} or RSK activities were determined by immune complex assays and compared with the enzyme activity from quiescent cells (lane 1).

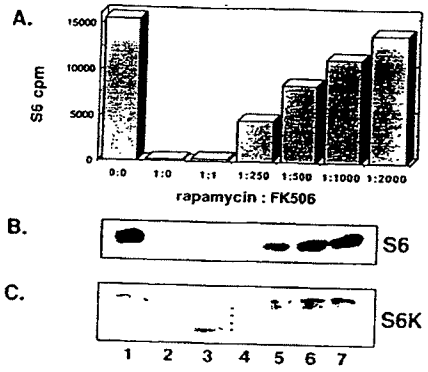

Figure 5. FK506 Antagonizes Inhibition of pp70^{S6K} Activity and Phosphorylation by Rapamycin

Quiescent Swiss 3T3 cells were preincubated for 30 min with different ratios of FK506 (0 to 8 μg/ml) and a single concentration of rapamycin (4 ng/ml). Cells were then stimulated with calf serum (10% [v/v]) for 10 min and lysed. pp70^{S6K} activities were measured by immune complex S6 phosphotransferase assays (B) and incorporation of ^{32}P into S6 quantitated by liquid scintillation and illustrated in bar graph form (A). Immunoprecipitates of pp70^{S6K} from this experiment were used for immunoblot analysis (C). Note the multiple bands of pp70^{S6K} (αII) identified by immunoblot analysis. At least four are denoted between lanes 3 and 4, indicating the existence of an unphosphorylated form (closed square) and at least three phosphorylated forms (dashes). Similar results were observed for the less abundant αI form of pp70^{S6K}.

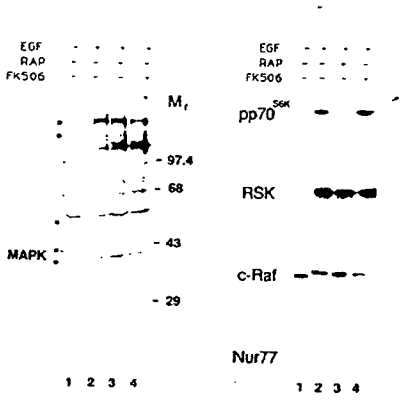

Figure 6. FK506 and Rapamycin Do Not Interfere with Tyrosine Phosphorylation or Phosphorylation of c-Raf, RSK, or Nur77

Left panel: Quiescent Swiss 3T3 cells were stimulated with EGF (25 ng/ml, 5 min; lanes 2–4) without or with pretreatment with rapamycin (20 ng/ml, lane 3) or FK506 (20 ng/ml, lane 4) for 10 min. Equal protein amounts of cell lysates were used for phosphotyrosine immunoblot analysis as described in Experimental Procedures. Phosphotyrosine antibodies (UBI) detected changes of tyrosine phosphorylation of molecular sizes approximately 42, 44, 57, 170, and >200 kd.

Right panel: Quiescent cells were similarly incubated with 10% calf serum, EGF, or immunosuppressants as described for the left panel. pp70^{S6K}, RSK, and Nur77 were immunoprecipitated from ^{32}P-labeled cell lysates stimulated with serum for 30 min as described (Chen et al., 1992). EGF-stimulated c-Raf phosphorylation was monitored by the appearance of a slow mobility form on SDS gels when examined by immunoblot analysis as described (Experimental Procedures and Wood et al., 1992). Biosynthetic labeling with ^{32}P followed by c-Raf immunoprecipitation yielded similar results (not shown).

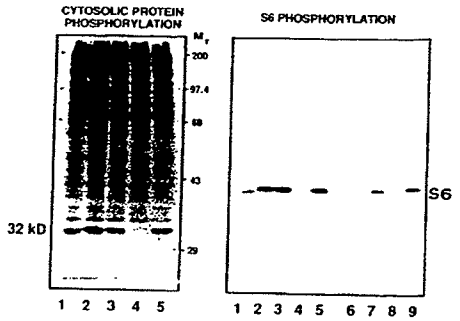

Figure 7. Effect of Rapamycin on the Phosphorylation of Cellular Proteins and the Ribosomal Protein S6 In Vivo

Quiescent Swiss 3T3 cells were biosynthetically labeled with inorganic ^{32}P for a total of 3 hr and lysed after serum stimulation for 1 hr (lanes 2–5 and 9) or 10 min (lanes 7 and 8). Cells were pretreated with or without rapamycin and/or FK506 for 30 min. Phosphorylated cytosolic proteins (left panel) or partially purified ribosomes (right panel) were separated by SDS–10% or 12% polyacrylamide gel electrophoresis, and phosphoproteins were detected by autoradiography. Lane 1, quiescent control; lane 2, cells were stimulated with 10% calf serum for 1 hr; lane 3, cells treated with 10% calf serum for 1 hr with pretreatment of FK506 (4 ng/ml); lane 4, cells treated with 10% calf serum for 1 hr with pretreatment of rapamycin (4 ng/ml); lane 5, cells stimulated with 10% calf serum for 1 hr with pretreatment of rapamycin (4 ng/ml) and FK506 (8 μg/ml). Lane 5 illustrates the antagonism of rapamycin effects on S6 phosphorylation by a 2000-fold excess of FK506. Lanes 6–9 are results from a separate experiment. Lane 6, quiescent control; lane 7, cells stimulated with 10% calf serum for 10 min; lane 8, cells stimulated with serum for 10 min following pretreatment with rapamycin (4 ng/ml); lane 9, cells stimulated with serum for 1 hr.

cal phosphorylation of the 40S ribosomal protein S6 (see Erikson, 1991; Sturgill and Wu, 1991). The apparent specificity of rapamycin toward pp70^{S6K} therefore allowed us to ascertain the contribution of this enzyme to mitogen-induced S6 phosphorylation. As shown in Figure 7, serum-stimulated (1 hr and 10 min) S6 phosphorylation in vivo (compare lane 1 with lane 2, and lane 6 to lanes 7 and 9) was completely blocked by rapamycin (lanes 4 and 8) but not by FK506 (lane 3). The ability of rapamycin to block S6 phosphorylation was reversed by excess FK506, again consistent with an FKBP-mediated process (lane 5). Thus, S6 phosphorylation was blocked even when RSK was maximally activated. Conversely, pp70^{S6K} activation, without RSK activation, results in S6 phosphorylation (Blenis et al., 1991). We therefore conclude that pp70^{S6K} and not RSK is the major cellular S6 kinase activated during the mitotic cell cycle.

Rapamycin inhibits the proliferation of yeast and some B and T lymphocytes. Given the specific inhibition of pp70^{S6K} by rapamycin in Swiss 3T3 cells, we utilized rapamycin to examine the role of the pp70^{S6K} signaling system in the regulation of fibroblast cell proliferation. Rapamycin and serum were added to Swiss 3T3 cells, and growth was monitored by changes in DNA synthesis and overall cell numbers. Changes in DNA synthesis were monitored following addition of serum plus rapamycin or FK506 to quiescent Swiss 3T3 cells with 1 hr pulses of [^{3}H]thymidine. Rapamycin significantly delayed entry into S phase for

serum-stimulated 3T3 cells (lengthened G1 phase) when compared with FK506 (Figure 8A) or serum-stimulated cells without drug addition (not shown). FK506 had little effect on G1 transition in these cells. In addition, the effect of rapamycin on cell growth was determined by cell counts. Rapamycin reduced the rate of serum-stimulated cell proliferation but did not inhibit the eventual attainment of saturation density, whereas FK506 had little effect in comparison with the serum-stimulated controls (Figure 8B).

Stimulation of pp70^{S6K}, RSK, and MAP kinase activities was also observed in phytohemagglutinin/phorbol myristate acetate–activated peripheral blood lymphocytes (PBLs; Figure 9 and not shown). In contrast to Swiss 3T3 fibroblasts, both FK506 and rapamycin significantly inhibited cell proliferation, by approximately 55% and 80%, respectively. Rapamycin completely blocked the activation of pp70^{S6K} but not of RSK. FK506 had no effect on either of these signaling systems.

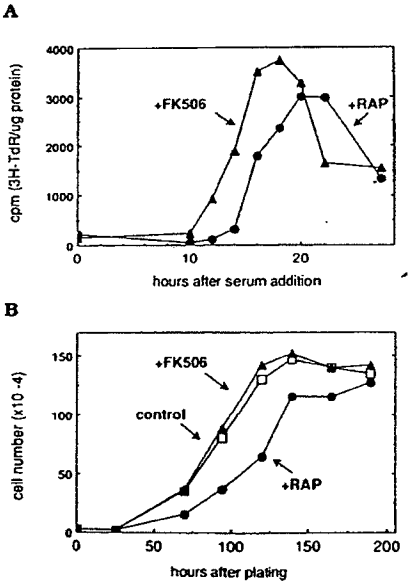

Figure 8. Rapamycin Delays the Onset of DNA Synthesis and Reduces the Rate of Cell Growth in Swiss 3T3 Cells

(A) Cells were plated (at 2.5 × 10^4 cells per 60 mm dish) and allowed to grow for 2 days. At approximately 50% confluence, medium was changed to low serum (0.5% [v/v]) DMEM for 2 additional days and then stimulated with 10% calf serum with the addition of FK506 (20 ng/ml, triangles) or rapamycin (20 ng/ml, circles). Cells were pulsed (1 hr) with [^{3}H]thymidine and harvested at 2 hr intervals to determine the incorporation of isotope into the DNA of growing cells. The results provided are mean values of duplicate measurements that were normalized for measured protein.

(B) Cells were plated (at 2.5 × 10^4 cells per 60 mm plate) and allowed to attach to the culture dishes for 5 hr. Cell cultures (in triplicate) were treated without (open squares) or with rapamycin (20 ng/ml, closed circles) or FK506 (20 ng/ml, closed triangles). Each set of cells was allowed to grow for the designated times and counted for cell number per plate. All values in the figure represent mean values of six cell counts for each time point from three plates.

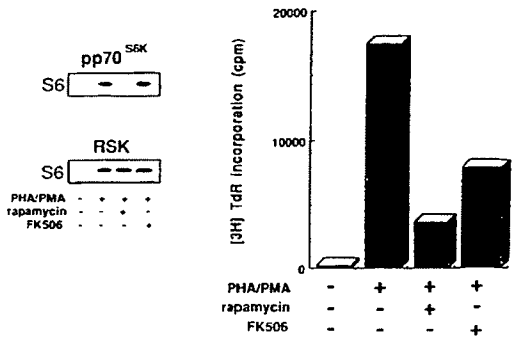

Figure 9. Rapamycin Antagonizes Activation of pp70^{S6K} and PBL Cell Proliferation

The pp70^{S6K} and RSK S6 phosphotransferase activities (left panels) and DNA synthesis (right panel) of highly purified PBLs were determined as described in Experimental Procedures. Cells were preteated for 5 min without or with rapamycin (5 ng/ml) or FK506 (5 ng/ml) and then stimulated for 45 min with phytohemagglutinin (PHA; 2.5 μg/ml) and phorbol myristate acetate (PMA; 20 ng/ml).

Discussion

FKBP homologs have been identified in bacteria, yeast, and higher eukaryotes, yet little about their cellular function is known. Owing to their ubiquitous nature, these receptors and their cellular ligands may play a general role in the control of cell growth. Recent progress in the molecular analysis of cyclosporin A and FK506, and their immunophilins, has provided new insight into the mechanism of action of these complexes. These studies have suggested a model whereby the interaction of immunosuppressant with immunophilin results in the binding of a third protein and/or complex, which acts as an effector for a signaling process. In the case of FK506 and cyclosporin A, the Ca^{2+}/calmodulin-dependent phosphatase calcineurin has been identified as the putative effector protein (Liu et al., 1991). The formation of this ternary complex and the extremely low concentrations of drug necessary to elicit a physiological response are consistent with the proposed gain-of-function model (McKeon, 1991; Schreiber, 1991). This model provides an explanation for the observed biological activity of drug when only a small percentage of the total cellular drug receptor is part of the complex. In contrast to what is known regarding FKBP–FK506, the mechanism whereby FKBP–rapamycin complexes work is poorly understood. It is likely that rapamycin's mechanism of action is the result of similar types of complex formations in which rapamycin positively or negatively influences distinct effector molecules. We have provided convincing evidence that the putative rapamycin-modulated effector molecules interfere with the growth-regulated pp70^{S6K} signaling system in animal cells.

Several conclusions are presented here. First, we show that rapamycin blocks the activation of pp70^{S6K} phosphotransferase activity mediated by tyrosine kinase growth factor receptors, by the *src* oncogene tyrosine kinase, by phorbol ester–activated protein kinase C, by ionophore-

dependent Ca^{2+} signaling, by G protein agonists, by heat shock–induced activation, and following inhibition of protein synthesis. Rapamycin does not block the activation of RSK or of the MAP kinases. Furthermore, FK506 does not block the activation of either of these signaling pathways. Rapamycin antagonized growth-dependent activation of $pp70^{S6K}$ in 3T3 fibroblasts, chicken embryo fibroblasts, HeLa cells, PC12 cells, and PBLs (Figures 1 and 9 and data not shown).

Second, inhibition of agonist-stimulated activation of $pp70^{S6K}$ was observed at very low concentrations of rapamycin and importantly, required binding to FKBP, as demonstrated by the fact that FK506 antagonizes rapamycin inhibition. These results are consistent with the block in $pp70^{S6K}$ activation being the result of a gain of function induced by rapamycin binding to FKBP.

Third, activation of $pp70^{S6K}$ by the reagents used in this study is accompanied by serine/threonine phosphorylation. In cells incubated with rapamycin, $pp70^{S6K}$ (αI and αII forms) is not phosphorylated. Two simple explanations are consistent with the gain-of-function hypothesis: FKBP–rapamycin inhibits an upstream $pp70^{S6K}$-activating kinase(s) or FKBP–rapamycin activates a phosphatase specific for $pp70^{S6K}$. Since FKBP–rapamycin complexes do not directly inhibit $pp70^{S6K}$ in in vitro kinase assays and since upstream kinases for $pp70^{S6K}$ have not been identified, we cannot presently determine whether upstream activating kinases are inhibited by rapamycin. Furthermore, unlike the FK506-induced binding and inactivation of calcineurin to FKBP (Liu et al., 1991), rapamycin does not appear to induce binding of $pp70^{S6K}$ to FKBP12 (Kuo et al., unpublished data). It is still possible that other FKBPs may interact directly with $pp70^{S6K}$. Notably, $pp70^{S6K}$, activated by several initially different signaling systems, is rapidly dephosphorylated/inactivated following rapamycin addition, with a half-life of approximately 2 min. These data are also consistent with the possible activation of a $pp70^{S6K}$-specific phosphatase. Phosphatase 2A has been previously shown to inactivate $pp70^{S6K}$ in vitro (Ballou et al., 1988). If rapamycin activates phosphatase 2A, then $pp70^{S6K}$ could be maintained in the dephosphorylated state. Addition of the phosphatase 2A– or 1C–specific inhibitor calyculin A or okadaic acid resulted in the phosphorylation and activation of $pp70^{S6K}$ as well as RSK. This result is consistent with one or both of these phosphatases being the cellular $pp70^{S6K}$ phosphatases. However, rapamycin blocked the $pp70^{S6K}$ but not RSK phosphorylation and activation by calyculin A. Thus, rapamycin does not appear to work via the activation of type 1C or 2A phosphatases. Furthermore, activation of $pp70^{S6K}$ following inhibition of protein tyrosine phosphatases with vanadate was also blocked by the addition of rapamycin. It is possible that rapamycin activates a calyculin A– or okadaic acid–insensitive phosphatase specific for both $pp70^{S6K}$ and the 40S ribosomal protein S6. This is unlikely, though, since distinct phosphatases have been suggested to dephosphorylate these phosphoproteins in vivo (Andres and Maller, 1989; Olivier and Thomas, 1990; Ballou et al., 1988), indicating that phosphorylation sites requiring phosphatases with distinct specificities must be activated by rapamycin. The data in Figures 6 and 7 indicate that a broad specificity phosphatase is not activated.

Fourth, rapamycin effects were specific for $pp70^{S6K}$ and did not interfere with the activation of the MAP kinase/RSK phosphorylation cascade. Immunoblot analysis with anti-phosphotyrosine or anti-Raf-1 antibodies from unstimulated and stimulated cells revealed that tyrosine phosphorylation and c-Raf phosphorylation were similarly not affected by rapamycin. Rapamycin also did not affect the activation of protein kinase C or of Ca^{2+}-regulated kinases, because phorbol esters or Ca^{2+} ionophores were still able to activate RSK. Furthermore, addition of [γ-^{32}P]ATP to cell-free lysates from treated and untreated cells revealed no significant differences in the various phosphotransferase activities observed under these conditions.

Fifth, a variety of in vitro S6 kinases have been identified, including protein kinase C and RSK. Since activation of these enzymes is not blocked by rapamycin, we examined its effects on S6 phosphorylation. Rapamycin completely blocked the serum-stimulated phosphorylation of S6. The phosphorylation of a variety of other major phosphoproteins was not affected by rapamycin. Previous studies have shown that activation of $pp70^{S6K}$ without RSK activation results in S6 phosphorylation (Blenis et al., 1991). This work provides the complementary experiment in which we have activated RSK and not $pp70^{S6K}$. These experiments establish $pp70^{S6K}$ as the major physiological, growth-responsive S6 kinase activated during the G1 phase in somatic cells.

Finally, the lack of toxicity and apparent specificity of rapamycin allowed us to investigate to what extent $pp70^{S6K}$ and S6 phosphorylation participate in the regulation of Swiss 3T3 cell proliferation. Addition of rapamycin, along with serum, to quiescent cells resulted in a significant delay in the entry of stimulated cells into S phase and reduced the rate of cell proliferation. Although cell growth was slowed, the final saturation density was nearly the same as in untreated cells. Thus, in Swiss 3T3 fibroblasts, the $pp70^{S6K}$ signaling system plays an ancillary, redundant role in the regulation of cell proliferation. However, in PBLs, the $pp70^{S6K}$ signaling system appears to play a more dominant role in cell growth, as the rapamycin-mediated antagonism of $pp70^{S6K}$ activation correlates with ~80% inhibition of cell proliferation. It is also worth noting that FK506 inhibited PBL proliferation by approximately 55% without affecting the activation of $pp70^{S6K}$, RSK, or MAP kinase activities (Figure 9 and not shown). Thus, FK506–FKBP–calcineurin complexes are modulating a distinct signaling system in PBLs, one that apparently does not play a major role in fibroblast cell growth.

Following activation of the *src* protein kinase in chicken embryo fibroblasts, $pp70^{S6K}$ is fully activated well into G1 (Blenis and Erikson, 1985). In serum-stimulated Swiss 3T3 fibroblasts, $pp70^{S6K}$ remains activated into late G1 phase of the cell cycle (Chen and Blenis, unpublished data). Since rapamycin has been proposed to inhibit yeast and T cell proliferation in late G1, the regulation of $pp70^{S6K}$ during this time may be crucial to growth control. S6 phosphorylation may participate in the regulation of protein synthesis (Erikson, 1991; Sturgill and Wu, 1991; and references therein).

The possibility exists that S6 phosphorylation in G1 may be necessary for the synthesis and/or accumulation of key regulatory proteins required for progression to S phase. Therefore, without S6 phosphorylation, the synthesis of these critical proteins would be slowed, resulting in a prolonged G1 transition as shown for Swiss 3T3 fibroblasts, or even the inability to traverse G1 as in T cell proliferation. Consistent with this hypothesis, the addition of rapamycin to IL-2-dependent D10 T cells into late G1 inhibits their proliferative response to IL-2 (Florentino and Crabtree, unpublished data).

Rapamycin is also a potent inhibitor of Saccharomyces cerevisiae cell proliferation, causing irreversible inhibition in the G1 phase of the cell cycle (Heitman et al., 1991). However, yeast homologs of pp70^{S6K} (and RSK) have not been identified, and genetic evidence indicates that S6 phosphorylation may have little effect on yeast cell proliferation (Johnson and Warner, 1987). Thus, it is also possible that rapamycin targets upstream pp70^{S6K} effectors that play a greater (or evolutionarily conserved) role in the regulation of cell proliferation. For example, if rapamycin activates a phosphatase activity, this could have targets other than pp70^{S6K}. Experiments are now underway to identify pp70^{S6K} upstream kinases and phosphatases and to determine the effects of rapamycin on their growth-regulated activities.

Experimental Procedures

Materials

Mouse EGF was purchased from Bethesda Research Laboratories, Inc. (Gaithersburg, MD). Calyculin A and okadaic acid were purchased from LC Services (Woburn, MA). Bombesin and A23187 were from Calbiochem (La Jolla, CA). Cycloheximide and phorbol myristate acetate were from Sigma (St. Louis, MO). Potato acid phosphatase was from Boehringer Mannheim (Indianapolis, IN). Ribosomal 40S subunits were purified from rat liver as described (Terao and Ogata, 1970), and recombinant chicken RSK protein was produced as previously described (Chung et al., 1991a). Tissue culture media and sera were purchased from GIBCO (Grand Island, NY). [γ-^{32}P]ATP and [methyl-^{3}H]thymidine were from New England Nuclear (Boston, MA), and ^{125}I-labeled protein A was from ICN (Irvine, CA).

Cell Cultures

Swiss 3T3 fibroblasts were cultured in Dulbecco's modified Eagle's medium (DMEM) supplemented with 5% (v/v) heat-inactivated fetal bovine serum and 5% (v/v) calf serum. Confluent plates were further cultured in DMEM containing 0.5% calf serum and 20 mM HEPES (pH 7.4) for 36–48 hr prior to experiments. CEF and CEF infected with NY72-4, a temperature-sensitive transformation mutant of Rous sarcoma virus, were cultured as described (Chen and Blenis, 1990).

PBLs were isolated as follows. Concentrated human blood (25 ml, Stanford Blood Center) from a healthy donor was layered onto 15 ml Ficoll-Hypaque cushions (Pharmacia) and centrifuged at room temperature (two times at 1500 rpm, 15 min, Beckman GPR). The lymphocyte layer was isolated and washed three times in phosphate-buffered saline (once at 1200 rpm and two times at 1000 rpm) and resuspended at 1 × 10^6 cells per ml in RPMI 1640, 10% fetal bovine serum, 100 U/ml penicillin and streptomycin (GIBCO). Cells were pretreated (5 min) with rapamycin (5 ng/ml), FK506 (5 ng/ml), or no immunosuppressant and then stimulated (45 min) with phytohemagglutinin (2.5 μg/ml) and phorbol myristate acetate (20 ng/ml), as appropriate. After 1 × phosphate-buffered saline wash, PBLs were lysed in buffer A (Kuo et al., 1991) with 0.2% NP-40, 0.1 mM Na_3VO_4, and 20 mM β-glycerophosphate and microfuged (15 s at 4°C). The supernatant (crude cytoplasmic fraction) was frozen in liquid N_2 and used for pp70^{S6K}, RSK, and MAPK assays. In parallel, aliquots of the PBLs (5 × 100 μl) were cultured for 40 hr and then pulsed with 1 μCi [^{3}H]thymidine for 8 hr. Cells were collected onto glass fiber filters, and quantitation of radioactivity was performed on a Matrix 96 direct beta counter (Packard).

Antibodies

pp70^{S6K} antibodies were generated against the predicted amino acids 20–39 or 502–525 of the pp70^{S6K} gene α1 (Grove et al., 1991). The generation and use of RSK antibodies have been described (Chen and Blenis, 1990). MAP kinase antisera were prepared against the predicted extreme carboxy-terminal 20 aa of the *erk*-1 gene (Boulton et al., 1990). The antibodies described above were used for immune complex kinase assays, immunoprecipitations, and immunoblotting analysis.

Immunoprecipitation and Protein Kinase Assays

Cell-free lysates and immunoprecipitations were prepared and protein kinase assays were performed in the immune complex as described (Chen and Blenis, 1990). MAP kinase antisera recognized both pp44$^{mapk/erk1}$ and pp42$^{mapk/erk2}$ in SDS-denatured lysates (Chen et al., 1992), but only pp44$^{mapk/erk1}$ under conditions maintaining native conformations (Wood et al., 1992). All MAP (recombinant RSK) kinase activities were also measured with a direct cell lysate kinase assay as described (Chung et al., 1991a, 1991b) with similar results. Phosphotransferase reactions were allowed to proceed for 15 min at 30°C (linear assay conditions). Conditions for immunoprecipitation of Nur77, c-Jun, or serum response factor from ^{32}P-labeled cells were as described (Chen et al., 1992).

Immunoblot Analysis

Samples were prepared as described above, and polypeptides were resolved by SDS–7.5% or 10% polyacrylamide gel electrophoresis and then transferred electrophoretically to nitrocellulose membranes in the transfer buffer (192 mM glycine, 25 mM Tris base) using a Hoefer tank blotter (50 V, 1.5 hr at 4°C). Following staining with Ponceau S to visualize the protein bands, destaining with several washes of water, and blocking in phosphate-buffered saline containing 0.2% Tween 20 and 2% bovine serum albumin (30 min each), the membrane was incubated for 1 hr in blocking buffer containing the carboxy-terminal pp70^{S6K} antiserum (1:500 dilution), antisera to c-Raf-1 (1:4000, see Wood et al., 1992), or antisera to phosphotyrosine (1:500, UBI or ICN). Membranes were washed three times with blocking buffer (10 min) at room temperature and further incubated in the same buffer containing ^{125}I-labeled protein A (0.1 μCi/ml) for an additional 1 hr. For anti-phosphotyrosine immunoblot analysis, membranes were incubated with anti-mouse immunoglobulin G rabbit antibodies (1:1500, Jackson Immuno Research) prior to addition of ^{125}I-labeled protein A. The membranes were then washed three times with phosphate-buffered saline containing 0.2% Tween 20 and air dried, followed by autoradiography.

Potato Acid Phosphatase Treatment

Dephosphorylation of pp70^{S6K} by potato acid phosphatase was completed as described previously (Chen and Blenis, 1990). Briefly, the immune-complexed enzymes were washed with cold buffer A and with phosphatase buffer. Heated or unheated potato acid phosphatase (1.5 U) was added to separate immune complexes resuspended in 50 μl of phosphatase buffer. The phosphatase reaction was continued for 30 min at 20°C and terminated by washing the immune complex with cold buffer B and ST buffer (Chen and Blenis, 1990). Enzymatic activities of dephosphorylated pp70^{S6K} were measured as described above, and actual dephosphorylation of the proteins was analyzed by immunoblot analysis.

In Vivo S6 Phosphorylation

Ribosomes were isolated from ^{32}P-labeled cultures as described (Blenis et al., 1991), and S6 proteins were further separated from other ribosomal subunit proteins in an SDS–12% polyacrylamide gel. Polypeptides in the gel were detected by Coomassie blue staining, and ^{32}P incorporation into S6 was determined by autoradiography.

Cell Proliferation

Swiss 3T3 fibroblasts (2.5 × 10^4) were plated on a 60 mm dish and grown for 2 days in DMEM with 10% fetal bovine serum. Cells were cultured for another 2 days in DMEM with 0.5% calf serum and 20 mM

HEPES (pH 7.4). After serum addition without or with pretreatment of FK506 (20 ng/ml) or rapamycin (20 ng/ml) for 30 min, cells were pulsed with [^{3}H]thymidine (2 μCi per plate) for 1 hr at various time points, fixed with cold 5% trichloroacetic acid solution, washed three times with cold STE buffer, and solubilized in 1 ml of 0.1% SDS, 0.01 N NaOH before an aliquot was taken for counting. Samples were counted in a Beckman liquid scintillation spectrometer, and results were normalized for protein concentrations determined by the BCA protein assay method (Pierce, Rockford, IL).

Cells plated in DMEM with 10% fetal bovine serum were allowed to attach on the plates for 5 hr and then incubated with or without immunosuppressants as described above. Cells were continuously cultured without any change of media, and the number of cells per plate was counted at 24 hr intervals. Trypsinized cells were resuspended in a known volume of DMEM and counted in a hemocytometer under a light microscope. Proliferation of PBLs was measured as described above.

Acknowledgments

We express our gratitude to R.-H. Chen, M. Monfar, and R. Tung for helpful comments during the preparation of this manuscript. We also thank our colleagues for various antibodies: T. Curran (c-Jun), L. Lau (Nur77), M. Greenberg (serum response factor), and T. Roberts and K. Wood (c-Raf). This research was supported by CA-46595 from the National Institutes of Health, by JFRA-257 from the American Cancer Society, and by the Lucille P. Markey Foundation (J. B.); and by the Howard Hughes Medical Institute and CA-39612 and HLB-33942 from the National Institutes of Health (G. R. C.). C. J. K. was supported by the Medical Scientist Training Program at Stanford University School of Medicine.

The costs of publication of this article were defrayed in part by the payment of page charges. This article must therefore be hereby marked "*advertisement*" in accordance with 18 USC Section 1734 solely to indicate this fact.

Received February 18, 1992; revised May 6, 1992.

References

Alcorta, D. A., Crews, C. M., Sweet, L. J., Bankston, L., Jones, S. W., and Erikson, R. L. (1989). Sequence and expression of chicken and mouse *rsk*: homologs of the *Xenopus laevis* ribosomal S6 kinase. Mol. Cell. Biol. *9*, 3850–3859.

Alvarez, E., Northwood, I. C., Gonzalez, F. A., Latour, D. A., Seth, A., Abate, C., Curran, T., and Davis, R. J. (1991). Pro-Leu-Ser/Thr-Pro is a consensus primary sequence for substrate protein phosphorylation. Characterization of the phosphorylation of c-*myc* and c-*jun* proteins by an epidermal growth factor receptor threonine 669 protein kinase. J. Biol. Chem. *266*, 15277–15285.

Andres, J. L., and Maller, J. L. (1989). Purification and characterization of a novel protein phosphatase highly specific for ribosomal protein S6. J. Biol. Chem. *264*, 151–156.

Ballou, L. M., Jeno, P., and Thomas, G. (1988). Protein phosphatase 2A inactivates the mitogen-stimulated S6 kinase from Swiss mouse 3T3 cells. J. Biol. Chem. *263*, 1188–1194.

Ballou, L. M., Luther, H., and Thomas, G. (1991). MAP2 kinase and 70K S6 kinase lie on distinct signalling pathways. Nature *349*, 348–350.

Banerjee, P., Ahmad, M. F., Grove, J. R., Kozlosky, C., Price, D. J., and Avruch, J. (1990). Molecular structure of a major insulin/mitogen-activated 70-kDa S6 protein kinase. Proc. Natl. Acad. Sci. USA *87*, 8550–8554.

Bierer, B. E., Mattila, P. S., Standaert, R. F., Herzenberg, L. A., Burakoff, S. J., Crabtree, G., and Schreiber, S. L. (1990a). Two distinct signal transmission pathways in T lymphocytes are inhibited by complexes formed between an immunophilin and either FK506 or rapamycin. Proc. Natl. Acad. Sci. USA *87*, 9231–9235.

Bierer, B. E., Somers, P. K., Wandless, T. J., Burakoff, S. J., and Schreiber, S. L. (1990b). Probing immunosuppressant action with a nonnatural immunophilin ligand. Science *250*, 556–559.

Blenis, J. (1991). Growth-regulated signal transduction by the MAP kinases and RSKs. Cancer Cells *3*, 445–449.

Blenis, J., and Erikson, R. L. (1985). Regulation of a ribosomal protein S6 kinase activity by the Rous sarcoma virus transforming protein, serum, or phorbol ester. Proc. Natl. Acad. Sci. USA *82*, 7621–7625.

Blenis, J., Chung, J., Erikson, E., Alcorta, D. A., and Erikson, R. L. (1991). Distinct mechanisms for the activation of the RSK kinase/MAP2 kinase/pp90^{rsk} and pp70-S6 kinase signaling systems are indicated by inhibition of protein synthesis. Cell Growth Diff. *2*, 279–285.

Boulton, T. G., Yancopoulos, G. D., Gregory, J. S., Slaughter, C., Moomaw, C., Hsu, J., and Cobb, M. H. (1990). An insulin-stimulated protein kinase similar to yeast kinases involved in cell cycle control. Science *249*, 64–67.

Chang, J. Y., Sehgal, S. N., and Bansbach, C. C. (1991). FK506 and rapamycin: novel pharmacological probes of the immune response. Trends Pharmacol. Sci. *12*, 218–223.

Chen, R.-H., and Blenis, J. (1990). Identification of *Xenopus* S6 protein kinase homologs (pp90^{rsk}) in somatic cells: phosphorylation and activation during initiation of cell proliferation. Mol. Cell. Biol. *10*, 3204–3215.

Chen, R.-H., Chung, J., and Blenis, J. (1991). Regulation of pp90^{rsk} phosphorylation and S6 phosphotransferase activity in Swiss 3T3 cells by growth factor-, phorbol ester-, and cAMP-mediated signal transduction. Mol. Cell. Biol. *11*, 1861–1867.

Chen, R.-H., Sarnecki, C., and Blenis, J. (1992). Nuclear localization and regulation of the *erk*- and *rsk*-encoded protein kinases. Mol. Cell. Biol. *12*, 915–927.

Chung, J., Chen, R.-H., and Blenis, J. (1991a). Coordinate regulation of pp90^{rsk} and a distinct protein-serine/threonine kinase activity that phosphorylates recombinant pp90^{rsk} in vitro. Mol. Cell Biol. *11*, 1868–1874.

Chung, J., Pelech, S., and Blenis, J. (1991b). Mitogen-activated Swiss mouse 3T3 RSK kinase I and II are related to pp44^{mpk} from sea star oocytes and participate in the regulation of pp90^{rsk} activity. Proc. Natl. Acad. Sci. USA *88*, 4981–4985.

Cobb, M. H., Boulton, T. G., and Robbins, D. J. (1991). Extracellular signal-regulated kinases: ERKs in progress. Cell Regul. *2*, 965–978.

Dumont, F. J., Melino, M. R., Staruch, M. J., Koprak, S. L., Fischer, P. A., and Sigal, N. H. (1990a). The immunosuppressive macrolides FK506 and rapamycin act as reciprocal antagonists in murine T cells. J. Immunol. *144*, 1418–1424.

Dumont, F. J., Staruch, M. J., Kiprak, S. L., Melino, M. R., and Sigal, N. H. (1990b). Distinct mechanisms of suppression of murine T cell activation by the related macrolides FK506 and rapamycin. J. Immunol. *144*, 251–258.

Erikson, E., and Maller, J. L. (1989). *In vivo* phosphorylation and activation of ribosomal protein S6 kinases during *Xenopus* oocyte maturation. J. Biol. Chem. *264*, 13711–13717.

Erikson, R. L. (1991). Structure, expression, and regulation of protein kinases involved in the phosphorylation of ribosomal protein S6. J. Biol. Chem. *266*, 6007–6010.

Flanagan, W. M., Corthesy, B., Bram, R. J., and Crabtree, G. R. (1991). Nuclear association of a T-cell transcription factor blocked by FK506 and cyclosporin A. Nature *352*, 803–807.

Grove, J. R., Banerjee, P., Balasubramanyam, A., Coffer, P. J., Price, D. J., Avruch, J., and Woodgett, J. R. (1991). Cloning and expression of two human p70 S6 kinase polypeptides differing only at their amino termini. Mol. Cell. Biol. *11*, 5541–5550.

Harding, M. W., Galat, A., Uehling, D. E., and Schreiber, S. L. (1989). A receptor for the immunosuppressant FK506 is a *cis-trans* peptidyl-prolyl isomerase. Nature *341*, 758–760.

Heitman, J., Movva, N. R., and Hall, M. N. (1991). Targets for cell cycle arrest by the immunosuppressant rapamycin in yeast. Science *253*, 905–909.

Johnson, S. P., and Warner, J. R. (1987). Phosphorylation of the *Saccharomyces cerevisiae* equivalent of ribosomal protein S6 has no detectable effect on growth. Mol. Cell. Biol. *7*, 1338–1345.

Jones, S. W., Erikson, E., Blenis, J., Maller, J. L., and Erikson, R. L. (1988). A *Xenopus* ribosomal protein S6 kinase has two apparent ki-

nase domains that are each similar to distinct protein kinases. Proc. Natl. Acad. Sci. USA *85*, 3377–3381.

Jurivich, D. A., Chung, J., and Blenis, J. (1991). Heat shock induces two distinct S6 protein kinase activities in quiescent mammalian fibroblasts. J. Cell. Physiol. *148*, 252–259.

Kozma, S. C., Ferrari, S., Bassand, P., Siegmann, M., Totty, N., and Thomas, G. (1990). Cloning of the mitogen-activated S6 kinase from rat liver reveals an enzyme of the second messenger subfamily. Proc. Natl. Acad. Sci. USA *87*, 7365–7369.

Kuo, C. J., Mendel, D. B., Hansen, L. P., and Crabtree, G. R. (1991). Independent regulation of HNF-1α and HNF-1β by retinoic acid in F9 teratocarcinoma cells. EMBO J. *10*, 2231–2236.

Liu, J., Farmer, J. D., Jr., Lane, W. S., Friedman, J., Weissman, I., and Schreiber, S. L. (1991). Calcineurin is a common target of cyclophilin-cyclosporin A and FKBP-FK506 complexes. Cell *66*, 807–815.

McKeon, F. (1991). When worlds collide: immunosuppressants meet protein phosphatases. Cell *66*, 823–826.

Morris, R. E. (1991). Rapamycin: FK506's fraternal twin or distant cousin? Immunol. Today *12*, 137–140.

Olivier, A. R., and Thomas, G. (1990). Three forms of phosphatase type 1 in Swiss 3T3 fibroblasts. J. Biol. Chem. *265*, 22460–22466.

Pulverer, B. J., Kyriakis, J. M., Avruch, J., Nikolakaki, E., and Woodgett, J. R. (1991). Phosphorylation of c-*jun* mediated by MAP kinases. Nature *353*, 670–674.

Schreiber, S. L. (1991). Chemistry and biology of the immunophilins and their immunosuppressive ligands. Science *251*, 283–287.

Siekierka, J. J., Hung, S. H. Y., Poe, M., Lin, C. S., and Sigal, N. H. (1989). A cytosolic binding protein for the immunosuppressant FK506 has peptidyl-prolyl isomerase activity but is distinct from cyclophilin. Nature *341*, 755–757.

Sturgill, T. W., and Wu, J. (1991). Recent progress in characterization of protein kinase cascades for phosphorylation of ribosomal protein S6. Biochim. Biophys. Acta *1092*, 350–357.

Sweet, L. J., Alcorta, D. A., and Erikson, R. L. (1990). Two distinct enzymes contribute to biphasic S6 phosphorylation in serum-stimulated chicken embryo fibroblasts. Mol. Cell. Biol. *10*, 2787–2792.

Terao, K., and Ogata, K. (1970). Preparation and some properties of active subunits from rat liver ribosomes. Biochem. Biophys. Res. Commun. *38*, 80–85.

Thomas, S. M., DeMarco, M., D'Arcangelo, G., Halegoua, S., and Brugge, J. S. (1992). Ras is essential for nerve growth factor– and phorbol ester–induced tyrosine phosphorylation of MAP kinases. Cell *68*, 1031–1040.

Wood, K. W., Sarnecki, C., Roberts, T. M., and Blenis, J. (1992). *ras* mediates nerve growth factor receptor modulation of three signal-transducing protein kinases: MAP kinase, Raf-1, and RSK. Cell *68*, 1041–1050.

termine if the structures we observed in nuclei of CIN-612 cells were indeed virions. Dot blot hybridization was performed on fractions from an isopycnic gradient purification (*17*) of HPV 31b virions produced in raft culture, and the presence of viral DNA was confirmed by Southern (DNA) blot hybridization (Fig. 4A). Lanes 6, 7, and 8 of Fig. 4A demonstrate the presence of HPV 31b DNA at low levels. From the copy number standards, we estimate the yield of viral particles to be at least 40 million per milliliter in lanes 7 and 8 (Fig. 4A). Fractions positive for HPV 31b DNA contained viral particles (Fig. 4B). The density gradient in fractions where virions were found was between 1.3 and 1.4 g/cm^3 as determined by weight. The presence of both HPV DNA and viral particles within the same fractions suggests that these are complete HPV virions, not empty capsids.

The ability to propagate papillomavirus in vitro is valuable not only for the understanding of the virus, but also for the eventual development of anti-viral treatments and the prevention of papillomavirus-induced lesions. These studies also establish the tight link between epithelial differentiation and HPV virion production. The ability of TPA to induce an increased expression of differentiation-specific markers suggests that a signal transduction pathway of epithelial differentiation has been identified. Virion production induced by phorbol esters has been described in other systems such as Epstein-Barr virus (*18*), Pichinde virus (*19*), Rift Valley fever virus (*20*), cytomegalovirus (*21*), and human immunodeficiency virus (*22*). The induction of the complete vegetative life cycle of HPVs in vitro requires both stratification at an air-liquid interface and protein kinase C (PKC) activation. In support of this hypothesis, the induction of viral particle biosynthesis by the addition of the synthetic diacylglycerol 1,2-dioctanoyl-*sn*-glycerol was observed (*23*). We believe that PKC activation of papillomavirus production is dependent on the induction of a more complex keratinocyte differentiation program and is not just a direct effect on capsid synthesis.

In this report, we described a system whereby latent infection of keratinocytes is converted into a productive infection leading to the formation of papillomavirus virions in culture. This tissue culture system will be useful in studies of the mechanisms whereby latency is maintained and terminated, and in the synthesis and assembly of papillomavirus virions.

REFERENCES AND NOTES

1. K. Syrjänen, L. Gissman, L. G. Koss, Eds., *Papillomaviruses and Human Disease* (Springer-Verlag, Berlin, 1987).
2. N. P. Salzman and P. M. Howley, Eds., *The Papillomaviruses*, vol. 2 of *The Papovaviridae* (Plenum, New York, 1987).
3. J. W. Kreider, M. K. Howett, A. E. Leure-Dupree, R. J. Zaino, J. A. Weber, *J. Virol.* 61, 590 (1987); J. W. Kreider, S. D. Patrick, N. M. Cladel, P. A. Welsh, *Virology* 177, 415 (1990).
4. J. Sterling, M. Stanley, G. Gatward, T. Minson, *J. Virol.* 64, 6305 (1990).
5. L. B. Taichman and R. F. LaPorta, in (*2*), pp. 109–140.
6. C. M. Meyers and L. A. Laimins, *Papillomavirus Rep.* 3, 1 (1992).
7. M. A. Bedell *et al.*, *J. Virol.* 65, 2254 (1991).
8. D. Asselineau, B. A. Bernard, C. Bailly, D. Darmon, M. Pruniéras, *J. Invest. Dermatol.* 86, 181 (1986).
9. R. Kopan, G. Traska, E. Fuchs, *J. Cell Biol.* 105, 427 (1987).
10. E. Fuchs and H. Green, *Cell* 19, 1033 (1980); R. Moll, W. W. Franke, D. L. Schiller, B. Geiger, R. Krepler, *ibid.* 31, 11 (1982); Y. J. Wu *et al.*, *ibid.*, p. 693; W. G. Nelson and T.-T. Sun, *J. Cell Biol.* 97, 244 (1983).
11. B. D. Ball, G. K. Walker, I. A. Bernstein, *J. Biol. Chem.* 253, 5861 (1978); B. A. Dale, K. A. Resing, J. D. Lonsdale-Eccles, *Ann. N.Y. Acad. Sci.* 455, 330 (1985); B. A. Dale, A. M. Gown, P. Fleckman, J. R. Kimball, K. A. Resing, *J. Invest. Dermatol.* 88, 306 (1987).
12. J. S. Rader *et al.*, *Oncogene* 5, 571 (1990).
13. Reproducible induction of differentiation occurred when raft cultures were incubated 16 to 24 hours every 4 days with cell culture medium that contained 16 nM TPA. Raft cultures were grown for 16 days then harvested, fixed in paraformaldehyde, embedded in paraffin, and sectioned for immunohistostaining (*23*).
14. H. Pfister and P. G. Fuchs, in (*1*), pp. 1–18.
15. C. Meyers and L. A. Laimins, unpublished material.
16. A. E. G. Dunn and M. M. Ogilvie, *J. Ultrastruct. Res.* 22, 282 (1968); C. R. Laverty, P. Russell, E. Hills, N. Booth, *Acta Cytol.* 22, 195 (1978); C. Morin and A. Meisels, *ibid.* 24, 82 (1980); J. Viac, D. Schmitt, J. Thivolet, *J. Invest. Dermatol.* 70, 263 (1978); S. Pilotti, F. Rilke, G. De Palo, G. Della Torre, L. Alasio, *J. Clin. Pathol.* 34, 532 (1981).
17. M. Favre, F. Breitburd, O. Croissant, G. Orth, *J. Virol.* 15, 1239 (1975).
18. D. H. Crawford and I. Ando, *Immunology* 59, 405 (1986); A. H. Davies, R. J. A. Grand, F. J. Evans, A. B. Rickinson, *J. Virol.* 65, 6838 (1991); Q. X. Li *et al.*, *Nature* 356, 347 (1992).
19. S. J. Polyak, W. E. Rawls, D. G. Harnish, *J. Virol.* 65, 3575 (1991).
20. R. M. Lewis, J. C. Morrill, P. B. Jahrling, T. M. Cosgriff, *Rev. Infect. Dis.* 11, 736 (1989).
21. B. G. Weinshenker, S. Wilton, G. P. A. Rice, *J. Immunol.* 140, 1626 (1988).
22. B. R. Cullen and W. C. Greene, *Cell* 58, 423 (1989); J. Laurence, H. Cooke, S. K. Sikder, *Blood* 75, 696 (1990).
23. C. Meyers and L. A. Laimins, in preparation.
24. D. J. McCance, R. Kopan, E. Fuchs, L. A. Laimins, *Proc. Natl. Acad. Sci. U.S.A.* 85, 7169 (1988).

25. We thank M. Turyk, G. Wilbanks, P. Larramendi, and S. Chou for assistance with electron microscopy, B. Roizman and S. Silverstein for critical reading of the manuscript, and the members of the L. Laimins laboratory for many helpful discussions. Supported by the Howard Hughes Medical Institute and a grant from the American Cancer Society (L.A.L.).

15 June 1992; accepted 15 July 1992

Rapamycin-Induced Inhibition of the 70-Kilodalton S6 Protein Kinase

Daniel J. Price,* J. Russell Grove,* Victor Calvo, Joseph Avruch, Barbara E. Bierer†

The immunosuppressant rapamycin inhibited proliferation of the H4IIEC hepatoma cell line. Rapamycin, but not its structural analog FK506, also inhibited the basal and insulin-stimulated activity of the p70 ribosomal protein S6 kinase. By contrast, insulin stimulation of the p85 Rsk S6 kinase and mitogen-activated protein (MAP) kinase activity were unaffected by drug. Rapamycin treatment of COS cells transfected with recombinant p70 S6 kinase completely inhibited the appearance of the hyperphosphorylated form of p70 S6 kinase concomitant with the inhibition of enzyme activity toward 40*S* subunits. Thus, rapamycin inhibits a signal transduction element that is necessary for the activation of p70 S6 kinase and mitogenesis but unnecessary for activation of p85 Rsk S6 kinase or MAP kinase.

Increased phosphorylation of multiple serine residues on the 40*S* ribosomal protein S6 numbers among the most rapid biochemical responses exhibited by cells stimulated with insulin or mitogens in vitro (*1*). Insulin or mitogen-stimulated S6 phosphorylation is catalyzed by one or both of two families of insulin or mitogen-activated S6 Ser-Thr protein kinases—the Rsk or p85 Rsk S6 kinases (*2*), and the p70 S6 kinases (*3*, *4*). Both families of S6 kinases are themselves regulated by Ser-Thr phosphorylation, although the immediate upstream regulators of the two S6 kinase families differ, at least in part. The *Xenopus* S6 kinase II, a p85 Rsk enzyme, is activated in vitro by phosphorylation with p42 MAP kinase (*5*). The MAP kinases are the dominant (perhaps only) immediate upstream activator of the p85 Rsk enzyme in situ in response to insulin or mitogens (*6*). Although the MAP kinases and cdc2 phosphorylate recombinant p70 S6 kinase in vitro in a putative regulatory

D. J. Price, J. R. Grove, J. Avruch, Diabetes Unit and Medical Services, Massachusetts General Hospital, Boston, MA, and Department of Medicine, Harvard Medical School, Boston, MA 02115.
V. Calvo, Division of Pediatric Oncology, Dana-Farber Cancer Institute and Harvard Medical School, Boston, MA 02115.
B. E. Bierer, Division of Pediatric Oncology, Dana-Farber Cancer Institute, Boston, MA; Hematology-Oncology Division, Department of Medicine, Brigham and Women's Hospital, Boston, MA; and Department of Medicine, Harvard Medical School, Boston, MA 02115.

*The first two authors contributed equally.
†To whom correspondence should be addressed.

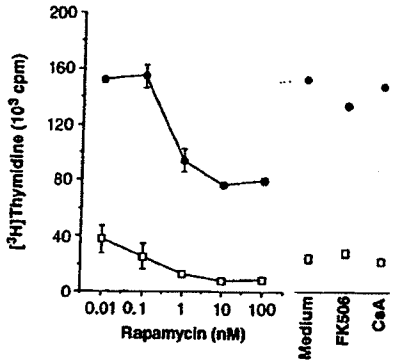

Fig. 1. Rapamycin-mediated inhibition of basal (□) and insulin-stimulated (●) proliferation of H4 rat hepatoma cells. Cells were grown to near-confluence in Swims S77 medium (Sigma) with fetal calf serum (5%) and horse serum (15%) at 37°C, 5% CO_2. Cells were cultured in serum-free medium 18 to 24 hours before assay. Serum-starved H4 cells were cultured in 96-well, flat-bottom plates (4 × 10^4 cells per well) in the absence (□) or presence (●) of 10^{-6} M insulin. CsA (100 nM), FK506 (100 nM), and rapamycin (as indicated) were added at the start of the assay. Proliferation was assessed by the incorporation of [^{3}H]thymidine during 16 hours after a 32-hour incubation. Mean ± SEM of triplicate determinations is shown, and this experiment is representative of four experiments.

domain (*7*), this phosphorylation is not sufficient to activate the p70 S6 kinase, indicating the existence of other, as yet unidentified, insulin-mitogen–activated p70 kinase–kinases (*7*).

The macrolide immunosuppressant rapamycin and its structural analog FK506 bind to the same family of intracellular receptors, termed FK506 binding proteins (FKBPs) (*8*). The complex of FK506 with FKBP binds to and inhibits the activity of calcineurin, a calcium-calmodulin–dependent Ser-Thr phosphatase (*9*). FK506, like the undecapeptide immunosuppressive agent cyclosporin A (CsA), inhibits T cell receptor–mediated events leading to lymphokine gene transcription (*10*). Rapamycin, but not FK506, inhibits lymphokine-dependent proliferation of cells at the G1 to S phase of the cell cycle (*10, 11*). The molecular target of rapamycin action has not been defined. We now demonstrate that the signal transduction pathway leading to the activation of p70 S6 kinase is selectively inhibited by rapamycin.

Rapamycin selectively inhibited the incorporation of [^{3}H]-labeled thymidine into serum-starved H4 hepatoma cells in a concentration-dependent fashion both in the presence of IC_{50}, half-maximal inhibitory concentration, of ~0.1 nM and absence of ~0.5 nM of the mitogen insulin (Fig. 1). Neither FK506 nor CsA, at 100-fold greater concentrations than those effective for rapamycin, inhibited basal or insulin-stimulated H4 proliferation (Fig. 1).

To analyze the rapamycin-mediated inhibition of H4 proliferation, we examined early biochemical events in insulin signal transduction. Insulin treatment of serum-starved H4 rat hepatoma cells results in the activation of cytosolic S6 protein kinases; assays of H4 cytosolic extracts showed a progressive increase in total S6 kinase to a plateau at 10 min that was sustained thereafter for at least 1 hour

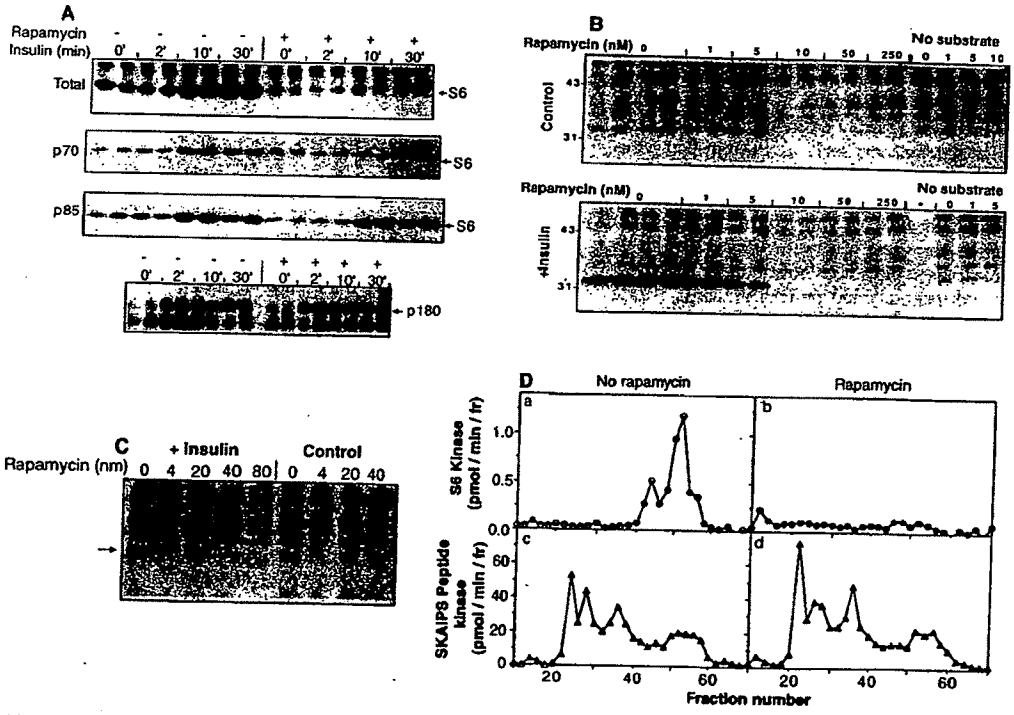

Fig. 2. Effect of rapamycin on insulin-regulated protein kinases in H4 hepatoma cells. (**A**) Serum-starved (24 hours) H4 cells were incubated in the presence or the absence of 20 nM rapamycin for 30 min before the addition of insulin (10^{-6} M). At the indicated times, cytosolic extracts were prepared. Aliquots of total extract (*20*) (top panel), extracts immunoprecipitated with affinity-purified polyclonal antibody to a peptide derived from p70 S6 kinase (*14*) (second panel), or p85 Rsk S6 kinase (third panel), were assayed for S6 kinase activity with 40*S* ribosomes as substrate. Bottom panel, proteins from H4 cell extracts Western-blotted with an antibody to phosphotyrosine. The region containing IRS-1 (P180) is shown. (**B**) Rapamycin-mediated inhibition of basal and insulin-stimulated S6 kinase activity. Rapamycin (0 to 250 nm) was added to serum-starved H4 cells 1 hour before harvest. Thirty minutes before harvest, the cells were either treated with insulin (10^{-6} M) or left untreated. Cells were harvested (*20*), and the kinase activity of cytosolic extracts detected as phosphorylation of 40*S* ribosomes (*7, 12*). (**C**) Effect of rapamycin on incorporation of ^{32}P into ribosomal protein S6 in intact H4 cells. Serum-starved (24 hours) H4 cells were incubated with serum-free medium containing 0.5 mCi of $^{32}P_i$ per 10-cm plate; after 1 hour, rapamycin (0 to 80 nm) was added. One hour later, insulin (10^{-6} M) was added to half of the plates. The cells were harvested 30 min later in extraction buffer (*20*) without Triton X-100, with aprotinin (10 U/ml) (0.5 ml per plate), and homogenized and centrifuged (10 min, 1000*g*). After further centrifugation (1.5 hours, 2 × 10^5*g*), sedimented material was subjected to SDS-PAGE. ^{32}P-labeled S6 is indicated by the arrow. (**D**) MonoQ chromatography of extracts from insulin-treated H4 cells. Serum-starved (24 hours) H4 cells were incubated in the absence (a and c) or the presence (b and d) of rapamycin (20 nM). After 30 min, insulin (10^{-6} M) was added to all plates. Cells were harvested 30 min thereafter into extraction buffer (*20*) without Triton X-100. Cytosolic extracts were chromatographed on a column (*23*). Fractions (fr) (1 ml) were assayed for kinase activities toward 40*S* ribosomes (a and b) and SKAIPS peptide (c and d) (*4, 7*).

(erk-1), expressed transiently in COS cells, exhibited similar regulatory behavior. The r-epi p85 Rsk S6 kinase and r-epi p44 MAP kinase were activated by treatment of cells with phorbol 12-myristate 13-acetate (PMA) or EGF, whereas the recombinant p70 S6 kinase was constitutively active, and the activity was not altered significantly by PMA, EGF (Fig. 3B), or withdrawal or readdition of serum (*15*). Treatment of COS cells with rapamycin abolished the activity of r-epi p70 S6 kinase, whereas the basal (*15*) or PMA-stimulated activities of the r-epi p85 S6 kinase and an r-epi p44 MAP kinase were not affected by 10- to 20-fold higher concentrations of rapamycin (Fig. 3C). Rapamycin treatment did not inhibit the expression or recovery of the r-epi p70 S6 kinase polypeptide (Fig. 3D). Moreover, the inhibition of p70 S6 kinase activity was specific for rapamycin; treatment of cells with a 100-fold higher concentration of FK506 failed to inhibit r-epi p70 S6 kinase activity (Fig. 3C).

The p70 S6 kinase is activated by phosphorylation at multiple Ser and Thr residues (*13*). Both the endogenous and recombinant p70 S6 kinase polypeptide expressed in COS cells appear as a ladder of polypeptide bands after SDS–polyacrylamide gel electrophoresis (PAGE), of which only those with the slowest mobility coelute on MonoQ chromatography with the active enzyme (*14*). The slowed mobility on SDS-PAGE is abolished by treatment with protein phosphatase and reflects a phosphorylation-induced conformational change associated with the active state. Although virtually all recombinant p70 S6 kinase polypeptides contain ^{32}P when isolated from ^{32}P-labeled COS cells, only a minority show the highly retarded migration on SDS-PAGE seen with purified active rat liver p70 S6 kinase, and coelute with S6 kinase activity. After an in vitro autophosphorylation reaction, this electrophoretically retarded fraction of p70 S6 kinase polypeptides appears as a highly phosphorylated species migrating more slowly than the bulk of p70 S6 kinase; the latter shows much lower incorporation of ^{32}P relative to its abundance (Fig. 3D). The inhibition of the p70 S6 kinase activity seen at increasing concentrations of rapamycin was correlated with the disappearance of the slowly migrating ^{32}P-labeled band observed after the autophosphorylation reaction in vitro. By contrast, the in vitro autophosphorylation associated with the faster migrating p70 polypeptide (Fig. 3D) and the overall ^{32}P incorporation occurring in situ into the faster migrating p70 polypeptides, which are catalytically inactive toward 40S subunits, were only diminished at much higher concentrations of rapamycin (*15*). Thus, rapamycin inhibition of p70 S6 kinase activity toward S6 in 40S subunits is paralleled by the selective loss of autophosphorylating activity associated with the fully active (slowest migrating) p70 S6 kinase species.

This result could be explained if rapamycin, alone or as a complex with an FKBP, bound to and inhibited only the active conformation of p70 S6 kinase or prevented the accumulation of the active conformation of p70 S6 kinase by preventing its activation or accelerating its dephosphorylation. The effect of rapamycin, alone and as a complex with FKBP12 (*17*), an FKBP known to bind rapamycin with high affinity (*8*), on the activity of purified, fully active rat liver p70 S6 kinase (*4, 14*) was examined in vitro. Rapamycin (40 nM), added either alone or after prebinding to an equimolar concentration of recombinant FKBP12, did not alter p70 S6 kinase activity, or the rate at which rat liver p70 S6 kinase was inactivated by phosphatase-2A (*15*). The lack of direct inhibition of active p70 S6 kinase by rapamycin and FKBP12 suggests either that another FKBP is required for rapamycin activity or that rapamycin inhibits p70 S6 kinase indirectly, by inhibiting an upstream activator that is also crucial for mitogenesis.

The mechanism by which insulin mediates activation of cytosolic p70 S6 kinase is incompletely understood. Intrinsic tyrosine kinase activity of the insulin receptor results in tyrosine phosphorylation of a 180-kD polypeptide substrate termed IRS-1 (*16*). Insulin-stimulated tyrosine phosphorylation of IRS-1 in H4 cells was not altered by concentrations of rapamycin that abolished p70 S6 kinase activity (Fig. 2B). Insulin activates an array of proline-directed protein kinases in H4 hepatoma cells, including MAP kinases and a form of cdc2 that phosphorylate a putative regulatory domain on intact p70 S6 kinase (*3, 7*). The activation of these enzymes can be monitored with a synthetic polypeptide substrate, SKAIPS peptide, corresponding to these Ser Pro/Thr Pro-rich p70 S6 kinase regulatory sequences (*7*). Rapamycin, at concentrations that completely inhibit activation of p70 S6 kinase, did not alter the activation of these SKAIPS peptide kinases in response to insulin (Fig. 2D), indicating that MAP kinase and cdc2 activities are unaffected by drug (*18*). Thus, the target for rapamycin appears to be situated downstream of the insulin receptor kinase and tyrosine phosphorylation of IRS-1 on a signal transduction pathway distinct from that mediating activation of the erk-1/erk-2 MAP kinases. In the interleukin-2–dependent CTLL-20 cell line, interleukin-2 stimulates, and rapamycin inhibits, S6 kinase activity, whereas the PMA-stimulated activities of p85 Rsk S6 kinases and p42 MAP kinases are not inhibited by rapamycin (*19*). Thus, the mechanism of rapamycin action in lymphoid cells is also likely to involve a ubiquitous signal transduction element shared with nonlymphoid lineages. The rapamycin target might be a proximate upstream activator of the p70 S6 kinase, such as an activating p70 S6 kinase-kinase or a regulator of such an enzyme, and appears to be a crucial element linking growth factor receptors to subsequent intracellular processes regulating proliferation.

REFERENCES AND NOTES

1. J. P. Gordon *et al.*, *Curr. Top. Cell. Regul.* 21, 89 (1982); R. L. Erikson, *J. Biol. Chem.* 266, 6007 (1991).
2. S. W. Jones *et al.*, *Proc. Natl. Acad. Sci. U.S.A.* 85, 3377 (1988); E. Erikson and J. L. Maller, *J. Biol. Chem.* 261, 350 (1986); D. A. Alcorta *et al.*, *Mol. Cell. Biol.* 9, 3850 (1989).
3. P. Banerjee *et al.*, *Proc. Natl. Acad. Sci. U.S.A.* 87, 8550 (1990); S. C. Kozma *et al.*, *ibid.*, p. 7365; P. Jeno, L. M. Ballou, I. Novak-Hofer, G. Thomas, *ibid.* 85, 406 (1988).
4. D. J. Price, R. A. Nemenoff, J. Avruch, *J. Biol. Chem.* 254, 13825 (1989).
5. T. W. Sturgill, L. B. Ray, E. Erikson, J. L. Maller, *Nature* 334, 715 (1988).
6. N. G. Ahn and E. Krebs, *J. Biol. Chem.* 265, 11495 (1990); N. Gomez and P. Cohen, *Nature* 353, 170 (1991); J. Chung, S. L. Pelech, J. Blenis, *Proc. Natl. Acad. Sci. U.S.A.* 88, 4981 (1988); C. B. Barrett, E. Erikson, J. L. Maller, *J. Biol. Chem.* 267, 4408 (1992); J. R. Grove, D. J. Price, P. Banerjee, M. Ahmad, A. Balasubramanyam, J. Avruch, unpublished observations.
7. D. J. Price, N. K. Mukhopadhyay, J. Avruch, *J. Biol. Chem.* 266, 16821 (1991); N. K. Mukhopadhyay *et al.*, *ibid.* 267, 3325 (1992).
8. S. Schreiber, *Science* 251, 283 (1991).
9. J. Liu *et al.*, *Cell* 66, 807 (1991); D. F. Fruman, C. Klee, B. E. Bierer, S. J. Burakoff, *Proc. Natl. Acad. Sci. U.S.A.* 89, 3686 (1992).
10. F. J. Dumont, W. Staruch, S. L. Koprak, M. R. Merlino, N. H. Segal, *J. Immunol.* 144, 251 (1990); B. E. Bierer *et al.*, *Proc. Natl. Acad. Sci. U.S.A.* 87, 9231 (1990).
11. S. M. Metcalf and F. M. Richards, *Transplantation* 49, 798 (1990); J. E. Kay *et al.*, *Immunology* 72, 544 (1991).
12. R. A. Nemenoff, J. R. Gunsalus, J. Avruch, *Arch. Biochem. Biophys.* 245, 196 (1986).
13. D. J. Price, J. R. Gunsalus, J. Avruch, *Proc. Natl. Acad. Sci. U.S.A.* 87, 7944 (1990).
14. J. R. Grove *et al.*, *Mol. Cell. Biol.* 11, 2159 (1991).
15. J. R. Grove, D. J. Price, B. E. Bierer, J. Avruch, unpublished data.
16. M. F. White, R. Maron, C. R. Kahn, *Nature* 318, 183 (1985); X. J. Sun *et al.*, *ibid.* 352, 73 (1991).
17. J. J. Siekierka, S. J. U. Ung, M. Poe, C. S. Lin, N. G. Sigal, *ibid.* 341, 755 (1989); M. H. Harding, A. Galat, D. E. Uehling, S. L. Schreiber, *ibid.*, p. 758; Y.-J. Jin, S. J. Burakoff, B. E. Bierer, *J. Biol. Chem.* 26, 10942 (1992).
18. Rapamycin failed to inhibit the total and Suc-1 precipitable histone H1 kinase activity in H4 cells, further suggesting that cdc2 activity is unaffected by drug.
19. V. Calvo, C. Crews, T. Vik, B. E. Bierer, *Proc. Natl. Acad. Sci. U.S.A.*, in press.
20. H4 hepatoma and COS cells were harvested by homogenization in an extraction buffer containing 10 mM potassium phosphate (pH 6.5), 1 mM EDTA, 5 mM EGTA, 10 mM $MgCl_2$, 2 mM dithiothreitol (DTT), 1 mM vanadate, 50 mM β-glycerophosphate, Triton X-100 (0.1%), 2 μM leupeptin, 2 μM pepstatin, 0.2 mM phenylmethylsulfonyl fluoride (PMSF). Extracts were centrifuged for 1.5 hours at $2 \times 10^5 g$ and matched for protein content before chromatography or immunoprecipitation. Immune complexes bound to protein A Sepharose were washed three times in extraction buffer containing 0.25 M NaCl, and once in 20 mM

(Fig. 2A) (*12*). Incubation of H4 cells with rapamycin for 1 hour before addition of insulin led to a dose-dependent inhibition of both basal and insulin-stimulated S6 kinase activity in the cytosolic extract that was essentially complete at 10 nM rapamycin (Fig. 2B). The rapamycin inhibition of cytosolic S6 kinase activity of H4 cells was accompanied by an inhibition of basal and insulin-stimulated phosphorylation of the ribosomal protein S6 in situ (Fig. 2C).

To determine whether the inhibition of total S6 kinase activity by rapamycin was a consequence of the inhibition of p70 or p85 Rsk S6 kinase, or both, we resolved cytosolic extracts by anion-exchange chromatography (Figs. 2D and 3A) and by immunoprecipitation (Fig. 2A). H4 cytosolic extracts contain a dominant peak of S6 kinase activity that was eluted from a MonoQ anion-exchange column near 0.25 M NaCl (Fig. 2D). This peak corresponds to the p70 S6 kinase (*13*), and recombinant p70 S6 kinase expressed in COS cells exhibits similar elution (*14*). This peak of S6 kinase activity was completely inhibited by rapamycin pretreatment (Fig. 2D). Rapamycin also caused loss of S6 kinase activity in immunoprecipitates prepared with antibodies to a peptide from the p70 S6 kinase (Fig. 2A). The p85 Rsk S6 kinase, which elutes from MonoQ between 0.05 and 0.1 M NaCl (Fig. 3A), contributes less than 5% of the total cytosolic S6 kinase activity in H4 cells (Fig. 2D). We examined the activity of p85 S6 kinase by immunoprecipitation with an antibody to a peptide from the p85 Rsk kinase protein; p85 Rsk S6 kinase underwent activation in response to insulin, peaking in activity at 10 min (Fig. 2A). Concentrations of rapamycin that caused maximal inhibition of mitogenesis (Fig. 1) and total inhibition of p70 S6 kinase activity (Fig. 2B) did not alter the time course or magnitude of the insulin activation of p85 Rsk S6 kinase (Fig. 2A).

We further evaluated the differential sensitivity of the p70 and p85 Rsk S6 kinases to inhibition by rapamycin by directly examining the activity of the recombinant S6 kinase expressed transiently in COS cells. COS cells endogenously expressed both p85 and p70 S6 kinase activities, which were separable by MonoQ anion-exchange chromatography and independently regulated (Fig. 3A). Active phorbol esters (Fig. 3A), serum, or epidermal growth factor (EGF), but not insulin, each stimulated the activity associated with the p85 Rsk kinase, but did not alter the activity of the p70 S6 kinase (*15*). The endogenous MAP kinase activity in COS cells was increased by the same stimuli that increased p85 Rsk S6 kinase activity (*15*). Recombinant epitope-tagged (r-epi) (*16*) versions of p70 S6 kinase, p85 Rsk S6 kinase, and rat p44 MAP kinase

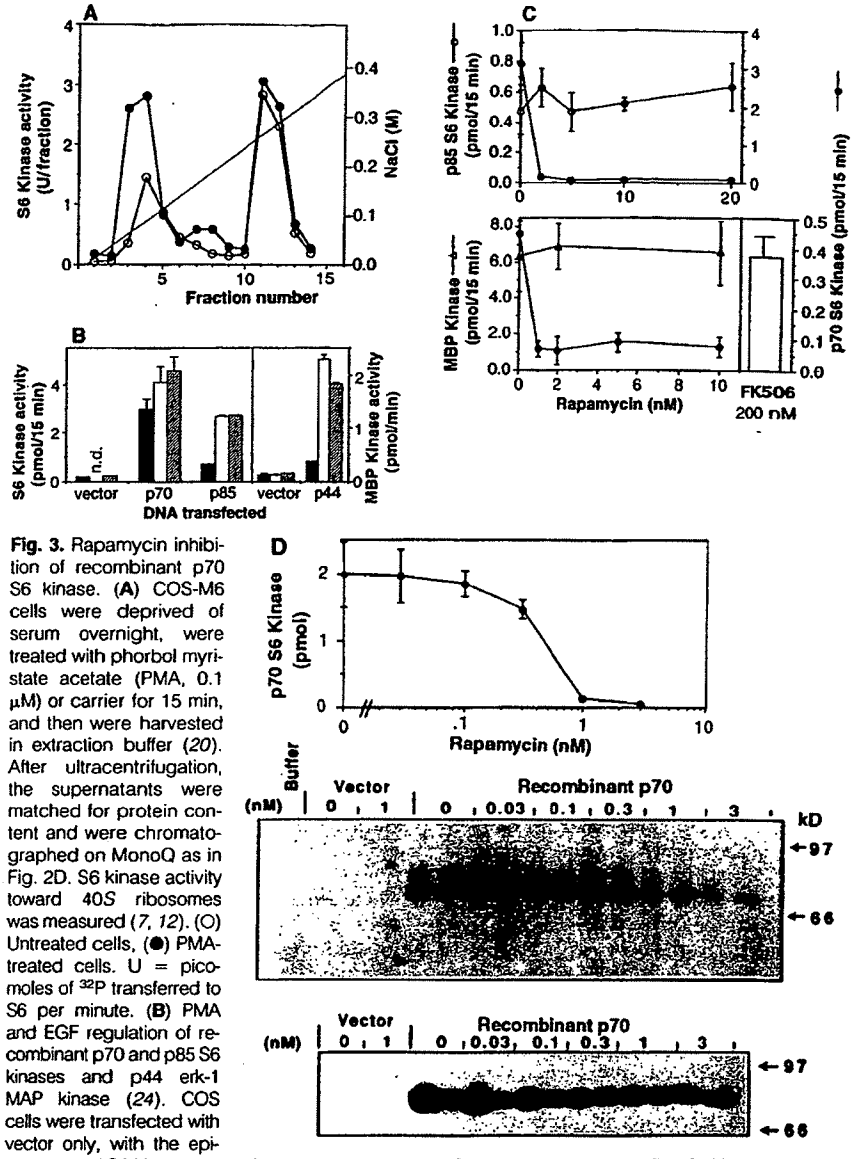

Fig. 3. Rapamycin inhibition of recombinant p70 S6 kinase. (**A**) COS-M6 cells were deprived of serum overnight, were treated with phorbol myristate acetate (PMA, 0.1 μM) or carrier for 15 min, and then were harvested in extraction buffer (*20*). After ultracentrifugation, the supernatants were matched for protein content and were chromatographed on MonoQ as in Fig. 2D. S6 kinase activity toward 40*S* ribosomes was measured (*7*, *12*). (○) Untreated cells, (●) PMA-treated cells. U = picomoles of ^{32}P transferred to S6 per minute. (**B**) PMA and EGF regulation of recombinant p70 and p85 S6 kinases and p44 erk-1 MAP kinase (*24*). COS cells were transfected with vector only, with the epitope-tagged S6 kinase expression constructs (r-epi p70 S6 kinase and r-epi p85 Rsk S6 kinase) or with the epitope-tagged p44 MAP kinase (r-epi erk-1) (*24*). After 24 hours, cells were left untreated (solid bars) or treated with PMA (100 nM) for 15 min (open bars) or EGF (60 ng/ml) for 10 min (hatched bars), then were homogenized in extraction buffer (*20*). Recombinant proteins were immunoprecipitated by incubation with the monoclonal antibody 12CA5 (*22*), and S6 kinase activity in the washed immunoprecipitates was determined (*7*, *12*). The r-epi erk-1 activity was assayed similarly with myelin basic protein (MBP) as substrate. Error bars indicate standard deviation ($n = 3$). (**C**) Recombinant p70 S6 kinase but not p85 S6 kinase or erk-1 is inhibited by rapamycin but not FK506. COS cells were transfected with r-epi p70 and r-epi p85 Rsk S6 kinase cDNAs (top panel), or r-epi p70 S6 kinase and r-epi erk-1 cDNAs (bottom panel); 48 hours later, the indicated concentrations of rapamycin were added to each plate 15 min before harvest. Recombinant proteins were immunoprecipitated and assayed for kinase activities as in Fig. 3B. Error bars indicate standard deviation (upper panel, $n = 5$; lower panel, $n = 6$). (**D**) Dose-response of rapamycin inhibition of r-epi p70 S6 kinase activity toward 40*S* subunits (top panel) (mean ± SD, $n = 6$) compared with r-epi p70 S6 kinase autophosphorylation (middle). COS cells were transfected with r-epi p70 S6 kinase cDNA. After 48 hours, rapamycin was added at the indicated concentrations. PMA (0.1 μM) was added 45 min later, and 15 min thereafter cells were extracted and were subjected to immunoprecipitation as in Fig. 3A. Autophosphorylation (middle panel) was measured by omitting the 40*S* subunits in the S6 kinase assay. The autoradiograph (middle) exhibits the ^{32}P incorporation into r-epi p70 polypeptide during a 15-min incubation with [γ-^{32}P]-labeled adenosine triphosphate. Portions of each immunoprecipitation were subjected to SDS-PAGE, were blotted onto PVDF membranes, and were probed with anti-p70 S6 kinase peptide antibody (*14*) (lower panel).

pranolol to block endogenous β-ARs). Cells expressing WT or Asn^{79} α_2ARs showed no obvious differences in their responses to the α_2AR antagonist idazoxan; idazoxan (100 nM) inhibited the maximum response to UK 14304 by 49 ± 8% (n = 8) in WT α_2AR cells and by 54 ± 6% (n = 10) in Asn^{79} α_2AR cells, and 1 μM idazoxan inhibited responses to agonists by 95 to 100% in both cell types. However, cells expressing the Asn^{79} α_2AR were one-sixth as sensitive to inhibition of the Ca^{2+} current by UK 14304 as cells expressing the WT α_2AR (Fig. 2C). These data suggest that the clonidine analog UK 14304 may behave as a partial agonist for Ca^{2+} current inhibition in comparison to clonidine or norepinephrine in these cells.

Modulation of K^+ or Ca^{2+} currents by α_2AR agonists or by somatostatin was mediated by means of PTX-sensitive G proteins. Incubation of AtT20 cells with PTX (100 ng/ml for 12 to 24 hours before recording) blocked agonist actions on both K^+ and Ca^{2+} currents. In PTX-treated cells, somatostatin (300 nM) increased K^+ currents in only 1 of 10 mock-transfected cells, 1 of 18 WT α_2AR cells, and 2 of 36 Asn^{79} α_2AR cells. Neither clonidine nor UK 14304 (1 to 10 μM) altered K^+ currents in any of these cells. Clonidine inhibited the Ca^{2+} current in only 1 of 35 WT α_2AR cells and 2 of 29 Asn^{79} α_2AR cells that had been treated with PTX.

Cells bearing either the WT or mutant Asn^{79} α_2AR coupled to inhibition of adenosine 3′,5′-monophosphate (cAMP) accumulation (*11*) through a PTX-sensitive pathway in AtT20 cells. Unlike the inhibition of Ca^{2+} currents, the potency of UK 14304 inhibition of cAMP accumulation was not reduced in cells with mutant α_2ARs (Table 1). Our observation that WT and Asn^{79} α_2ARs couple to inhibition of cAMP accumulation and suppression of Ca^{2+} currents through a PTX-sensitive pathway implies that these receptors can productively interact with G proteins mediating these two effector responses. However, when receptor coupling to G proteins was evaluated by guanine nucleotide modulation of agonist binding (*12*), this coupling was less for Asn^{79} α_2ARs than for WT α_2ARs (Table 1).

These data are consistent with observations for the α_2AR (*2*, *3*) that suggest that mutation of Asp^{79} perturbs G protein–dependent agonist interactions but not G protein–independent antagonist interactions with the α_2AR. Perturbation of G protein-

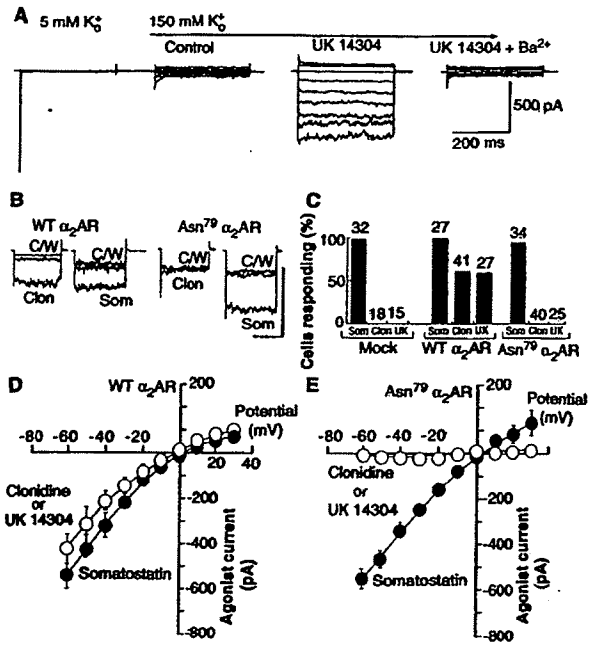

Fig. 1. Activation of K^+ currents by transfected α_2ARs and endogenous somatostatin receptors in AtT20 cells. **(A)** Depiction of superimposed traces of K^+ currents elicited by four sequentially increasing depolarizing pulses, six similar hyperpolarizing pulses applied in 5 mM external K^+ (K_o^+) and after switching from 5 mM K_o^+ to 150 mM K_o^+ (control) after addition of UK 14304 (1 μM) and after Ba^{2+} (1 mM) was added to the UK 14304–containing solution. Holding potential in 5 mM K_o^+ was −70 mV, and in 150 mM K_o^+ it was 0 mV (the K^+ equilibrium potential); large downward transient seen in 5 mM K_o^+ is the fast Na^+ current. **(B)** K^+ currents evoked by a 40-mV hyperpolarizing pulse from 0 mV in 150 mM K_o^+ solution in cells expressing WT α_2ARs and Asn^{79} α_2ARs; each set of traces consists of superimposed currents recorded in control (C) solution in the presence of agonist and after washout (W). Somatostatin (Som, 100 nM) and clonidine (Clon, 100 nM) were added to WT α_2AR cells; these agonists were added at a final concentration of 100 nM and 10 μM in Asn^{79} α_2AR cells. Calibrations are as in (A). **(C)** Percent of cells that exhibited an increased K^+ conductance in response to application of somatostatin (Som), clonidine (Clon), or UK 14304 (UK) in mock-transfected, WT α_2AR–expressing, and Asn^{79} α_2AR–expressing cells; numbers above each bar are numbers of cells examined. **(D** and **E)** Summary of agonist-induced K^+ current recorded in AtT20 cells transfected with the WT α_2AR (D) and the Asn^{79} α_2AR (E) mutant. Currents recorded in high-concentration K_o^+ solution (control) were subtracted from currents recorded in 100 nM somatostatin (closed circles) and 1 μM clonidine or UK 14304 (open circles). Each point in (D) is mean ± SEM from 14 experiments; points in (E) are from nine experiments.

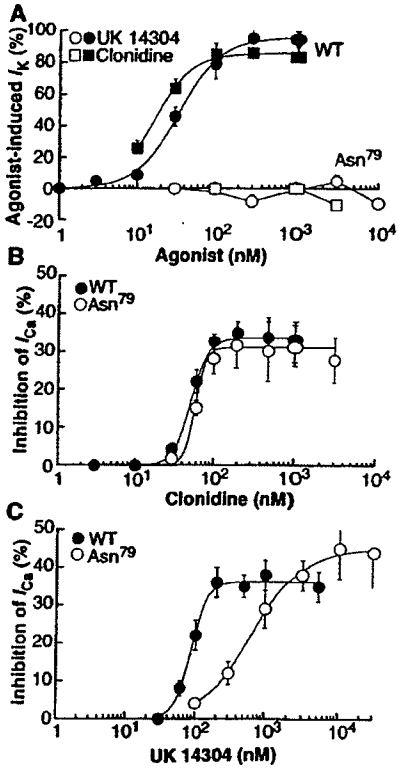

Fig. 2. Actions of AR agonists on K^+ currents (I_K) and Ca^{2+} currents (I_{Ca}) in AtT20 cells transfected with WT α_2ARs (filled symbols) or Asn^{79} α_2ARs (open symbols). **(A)** UK 14304 (circles)– and clonidine (squares)–induced increase in K^+ current in response to a 60-mV hyperpolarizing command (Fig. 1B); we normalized results by expressing them as a percentage of response produced by somatostatin (100 nM). Each point is mean ± SEM from six to eight cells for those expressing WT α_2ARs and four to five cells for those expressing Asn^{79} α_2ARs. Somatostatin EC_{50} values were 15 nM and 22 nM in cells expressing WT and Asn^{79} α_2ARs, respectively, and these values were not significantly different (student's t test). **(B** and **C)** Concentration-response curves for inhibition of I_{Ca} by clonidine (B) and UK 14304 (C); inhibition was measured as percent inhibition of the current elicited by depolarizing the cell from −70 mV to +20 mV. Each point is mean ± SEM [n = 15 for each point in (B); in (C), n = 12 for each point from WT α_2AR cells, and n = 8 to 10 for each point from Asn^{79} α_2AR cells]. EC_{50} values for somatostatin inhibition of I_{Ca} were 30 and 52 nM in WT α_2AR and Asn^{79} α_2AR cells, respectively, and these values were not significantly different (student's t test).

Tris Hcl (pH 7.4), 1 mM EGTA, 2 mM EDTA, 2 mM DTT, 10 mM β-glycerophosphate, Triton X-100 (0.1%), glycerol (10%), before assay of S6 kinase activity.

21. P. Banerjee, J. R. Grove, J. Kyriakis, J. Avruch, unpublished observations.
22. J. Field *et al.*, *Mol. Cell. Biol.* 8, 2159 (1988).
23. Cystolic extracts were matched for protein content, diluted with three parts of chromatography buffer [50 mM, β-glycerophosphate (pH 7.2), 1 mM DTT, 1 mM EGTA, 0.1 mM vanadate and applied to a MonoQ HR (515) column]. The column was eluted with a 90-ml gradient of NaCl (0 through 0.4 M final) in chromatography buffer.
24. The cDNA encoding rat p70 S6 kinase α1 (*14*), rat p85 S6 kinase (*3*), and rat erk-1 (*21*) were modified by insertion of a nine amino acid–peptide epitope derived from influenza virus hemagglutinin (*22*) at the NH_2-terminus of each polypeptide, immediately after the initiator methionine....
25. Supported in part by grants from PHS (RO1 DK17776), the American Cancer Society (BE-6), and the National Cancer Institute (PO1 CA39542). J.R.G. is a Capps Scholar in Diabetes from Harvard University. B.E.B. is the recipient of an Established Investigator Award from the American Heart Association. We thank D. Brautigan for purified phosphatase-2A, S. Pelech for antibodies to Rsk, and M. Chambers for secretarial support.

15 April 1992; accepted 30 June 1992

A Point Mutation of the α_2-Adrenoceptor That Blocks Coupling to Potassium But Not Calcium Currents

Annmarie Surprenant,* Debra A. Horstman, Hamid Akbarali, Lee E. Limbird

The α_{2A}-adrenergic receptor (adrenoceptor) was stably expressed in AtT20 mouse pituitary tumor cells; adrenoceptor agonists inhibited adenylyl cyclase, inhibited voltage-dependent calcium currents, and increased inwardly rectifying potassium currents. An aspartic acid residue (Asp^{79}) highly conserved among guanine nucleotide–binding protein (G protein)–coupled receptors was mutated to asparagine; in cells transfected with the mutant α_2-receptor, agonists inhibited adenylyl cyclase and calcium currents but did not increase potassium currents. Because distinct G proteins appear to couple adrenoceptors to potassium and calcium currents, the present findings suggest that the mutant α_2-adrenoceptor cannot achieve the conformation necessary to activate G proteins that mediate potassium channel activation.

The α_2-adrenergic receptors (α_2ARs) belong to the superfamily of G protein–coupled receptors, specifically to the branch of this family consisting of receptors coupled to the inhibition of adenylyl cyclase, the inhibition of Ca^{2+} currents, and the activation of K^+ currents by pertussis toxin (PTX)–sensitive G proteins (*1*). One or both of these latter two effects is responsible for the immediate inhibition of neurotransmitter release and neuronal firing produced by activation of presynaptic and postsynaptic α_2ARs on mammalian neurons (*1*). Multiple α_2AR subtypes have been identified by both pharmacological and molecular biological approaches, and site-directed mutagenesis of α_2ARs has identified several amino acids in transmembrane regions II through V as sites of interaction for agonist binding and for receptor coupling to the inhibition of adenylyl cyclase (*1*, *2*). However, it is not known whether cloned α_2ARs, when expressed in a heterologous system, can couple to diverse ion channels or whether specific domains can be identified that participate in coupling to specific diverse effector systems. We investigated the coupling of a stably transfected α_{2A}AR (*3*) to K^+ currents, Ca^{2+} currents, and adenylyl cyclase and the consequences of a single amino acid mutation [converting aspartic acid to asparagine at position 79 (Asn^{79} α_2AR)] on the coupling to these three effector systems.

The AtT20 cell does not express endogenous α_2ARs (Table 1) but contains somatostatin receptors that couple to inhibition of adenylyl cyclase (*4*), inhibition of Ca^{2+} currents (*5*), and activation of an inwardly rectifying K^+ current (*6*). Thus, we used AtT20 cells to evaluate the functional properties of wild-type (WT) α_2ARs or Asn^{79} α_2ARs. We compared somatostatin-induced alterations in K^+ and Ca^{2+} currents (*7*) with responses to the α_2AR agonists clonidine and UK 14304 in permanent transformants of AtT20 cells expressing recombinant WT or Asn^{79} α_2ARs (*8*).

The α_2AR agonist UK 14304 increased the K^+ current in cells expressing the WT α_2AR (Fig. 1); 95% of the current induced by UK 14304 was blocked by 1 mM Ba^{2+} (Fig. 1A), as would be expected if the agonist were opening inwardly rectifying K^+ channels (*9*). Somatostatin (100 nM) increased this current by two- to tenfold in all mock-transfected cells and in cells transfected with the WT α_2AR or Asn^{79} α_2AR (Fig. 1, B through E). Maximally effective concentrations of UK 14304 or clonidine produced a 1.5- to 8-fold increase in K^+ current in cells expressing the WT α_2AR (Fig. 1, B through D). Concentrations of clonidine and UK 14304 that produced half-maximal activation (EC_{50}) of the K^+ current were 14 and 30 nM, respectively, in cells expressing the WT α_2AR (Fig. 2A); these are similar to the EC_{50} values for the inwardly rectifying K^+ conductance activated by pharmacologically characterized α_{2A}ARs in autonomic enteric and central locus coeruleus neurons (*10*). The actior of maximally effective concentrations somatostatin and AR agonists were not additive (n = 22), which is evidence that the transfected WT α_2AR couples to the same set of K^+ channels as does the endogenous somatostatin receptor. In contrast to the WT α_2AR, the mutant Asn^{79} α_2AR did not activate K^+ currents (Fig. 1, B, C, and E), even in the presence of 10,000-fold higher concentrations of clonidine or UK 14304 (Fig. 2A).

In contrast to their effects on K^+ currents, α_2AR agonists were effective in inhibiting Ca^{2+} currents in AtT20 cells expressing WT α_2ARs or Asn^{79} α_2ARs (Fig. 3). In either case, the inhibition of Ca^{2+} currents by AR agonists was not quantitatively different from the inhibition of Ca^{2+} currents by somatostatin acting at endogenous receptors (Fig. 3, A and B). Somatostatin inhibits two high-voltage–activated (HVA) Ca^{2+} currents in AtT20 cells, a dihydropyridine-sensitive (HVA/L-typ current and a dihydropyridine-insensitive (HVA/N-type) current (*5*); α_2AR agonists similarly inhibited HVA/L- and HVA/N-type Ca^{2+} currents in cells expressing either WT or Asn^{79} α_2ARs (Fig. 3, C and D). Somatostatin inhibited the Ca^{2+} current in 92% of mock-transfected cells examined but inhibited Ca^{2+} currents in only 50% of cells expressing WT α_2ARs or Asn^{79} α_2ARs (Fig. 3B). The percentage of cells in which somatostatin inhibited the Ca^{2+} current was not correlated with the cell cycle nor the time after cell passage. The explanation for this observation is unclear because the percentage of cells responding to somatostatin with an increase in K^+ current was similar in all cells (Fig. 1C).

There were no apparent differences in the concentration-response curves for clonidine-induced inhibition of the Ca^{2+} current in cells expressing WT or Asn^{79} α_2ARs (Fig. 2B) or the norepinephrine-mediated responses (measured in the presence of pro-

A. Surprenant, Vollum Institute, Oregon Health Sciences University, Portland, OR 97201.
D. A. Horstman and L. E. Limbird, Department of Pharmacology, Vanderbilt University, Nashville, TN 37232.
H. Akbarali, Department of Medical Physiology, University of Calgary, Calgary, Alberta, Canada T2N 4N1.
*To whom correspondence should be addressed.

DOI: 10.1111/j.1540-8183.2009.00450.x

XIENCE V™ Stent Design and Rationale

NI (NADINE) DING, PH.D., STEPHEN D. PACETTI, M.S., FUH-WEI TANG, PH.D., MANISH GADA, M.S., and WOUTER ROORDA, PH.D.

From Abbott Vascular, Inc., 3200 Lakeside Drive, Santa Clara, California

Drug-eluting stents (DES) are a preferred treatment modality for occlusive coronary artery disease. First-generation DES have demonstrated high levels of efficacy. However, concerns have been raised over late thrombotic events. XIENCE V™ everolimus-eluting coronary stent is a second-generation DES designed to be more deliverable and safe, while maintaining efficacy in a broad patient population compared with first-generation DES.[1–3] As a drug/device combination product, the overall performance of a DES is determined by its components and how well they are integrated. XIENCE V utilizes the MULTI-LINK VISION® stent, the antiproliferative drug everolimus, a fluorinated polymer drug carrier, poly(vinylidene fluoride-co-hexafluoropropylene) (PVDF-HFP), and a stent-specific delivery system. A DES coating must fulfill the multiple goals of biocompatibility, controlled drug release and maintenance of the coating durability through stent crimping, and expansion in vivo. The XIENCE V coating utilizes a two-layer coating system composed of an acrylate primer and a fluorinated copolymer drug reservoir. Fluorinated polymers have a long history of use in permanent vascular implant applications. The XIENCE V fluorinated copolymer offers in vivo biocompatibility combined with excellent chemical stability and high purity. Described in this article are the design rationale and polymer selection criteria. The hemocompatibility and biocompatibility of the fluorinated polymer coating are discussed. Characterization results on drug release control, possible drug release mechanism, coating integrity, coating uniformity, and fatigue resistance are also presented. (J Interven Cardiol 2009;22:S18–S27)

Introduction

The rapid acceptance of first-generation drug-eluting stents (DES) when introduced, combined with the more recent concerns over late stent thrombosis, has driven the industry to develop second-generation DES. The goals for second-generation DES are to offer an optimal balance of safety, effectiveness, and deliverability in broad patient populations. Abbott Vascular's XIENCE V everolimus-eluting coronary stent system was designed with the intent of meeting these goals. Through extensive polymer screening, multiple coating design iterations, and extensive preclinical studies, the XIENCE V DES configuration was finalized with four major components, that is, the proven MULTI-LINK VISION stent and stent delivery system, the antiproliferative agent everolimus, and a fluorinated copolymer drug carrier.

Address for reprints: Nadine Ding, Ph.D., Fellow, Abbott Vascular, Inc., 3200 Lakeside Drive, Santa Clara, CA 95054. Fax: 408-845-3689; e-mail: ni.ding@av.abbott.com

Stent and Stent Delivery System

The MULTI-LINK VISION stent is made from a cobalt-chromium (Co-Cr) alloy. With a strut thickness of 81 μm, it has thinner struts than a stainless steel stent while still achieving excellent radiopacity and radial strength. The open cell and nonlinear link design makes the stent flexible and conformable to the vessel. Due to the thin struts, and optimized delivery system, the MULTI-LINK VISION system has a low profile at 0.040″ (1.0 mm) for a 3.0 × 18 mm stent, which enhances deliverability. The ML VISION stent delivery balloon is made of semicompliant polyether block amide (PEBAX®) material with short tapers and is designed to minimize injury outside of the stented region.

Drug

The drug everolimus, manufactured by Novartis Pharma AG, is a potent antiproliferative agent that acts on a wide range of cell types, including vascular smooth muscle cells, which it inhibits at a low nanomolar level ($IC_{50} = 0.9–3.6$ nM for bovine smooth muscle cells) in the G_1 phase of the cell cycle.[4] Everolimus is lipophilic, with an octanol/water partition coefficient of approximately 10.[4] The combination of smooth muscle cell inhibition, high potency, and high lipophilicity makes the drug an attractive candidate for controlled delivery from a DES for the prevention of neointimal hyperplasia. Multiple preclinical studies led to the selection of a low drug dose of 100 $\mu g/cm^2$ for the XIENCE V system. The XIENCE V stent releases approximately 80% of the drug in 1 month with near 100% drug release by 4 months. Details of preclinical pharmacokinetics are discussed in a separate article in this supplement issue. This drug dose is the lowest of all the commercialized "olimus" DES products.

XIENCE V Coating

The coating polymer plays a pivotal role in DES. Many factors need to be considered in selecting a polymer or polymer system. These include the hemocompatibility and biocompatibility of the polymer, polymer purity, coating integrity, polymer-drug miscibility, polymer processability, ability to control the drug release, and the stability (shelf-life) of the system. The XIENCE V system utilizes a two-layer coating construct composed of a primer layer and a drug-polymer reservoir layer with no topcoat. Poly(n-butyl methacrylate) (PBMA) is used as the thin, primer adhesion layer, and the drug reservoir layer is composed of poly(vinylidene fluoride-co-hexafluoropropylene) (PVDF-HFP) combined with everolimus. This two-layer coating construct is designed to ensure excellent adhesion of the drug matrix to the stent, while minimizing unwanted adhesions to the delivery balloon. The drug reservoir layer holds the drug onto the stent, controls the drug release, and contributes to the blood and vascular tissue compatibility of the DES stent. The following discussion will focus on the design rationale, the biocompatibility of the system, and the bench characterization results.

XIENCE V Formulation and System Integration

PVDF-HFP is a fluorinated copolymer of vinylidene fluoride and hexafluoropropylene with a molecular weight of 254–293 K Daltons as measured by gel permeation chromatography (GPC) (Fig. 1).

Unlike many fluorinated polymers, for example, polytetrafluoroethylene (PTFE), PVDF-HFP is soluble in select solvents, rendering it suitable for coating applications. Everolimus and PVDF-HFP are dissolved in a solvent system designed for high solvency, good coating quality, and complete solvent removal. The ratio of everolimus to PVDF-HFP is 17/83 (w/w) in the coating formulation. After the primer coating is applied, the drug-polymer solution is conformally coated. The final coating contains 100 μg drug per cm^2 of stent surface area.

Similar to many fluorinated polymers, the PVDF-HFP has low surface tension[5] and its coating is lubricious and nonsticky, which minimizes unwanted adhesion to the balloon and between struts. A PBMA primer layer assures good adhesion of the PVDF-HFP coating to the stent. PBMA has been utilized in other blood-contacting permanent implants[6] and adheres well to the metal oxide layer on the stent surface via a combination of noncovalent hydrophobic, polar, and hydrogen bonding interactions. PBMA is partially miscible with PVDF-HFP. Hence, the adhesion of the PVDF-HFP drug reservoir to the primer layer is high as the PBMA and PVDF-HFP polymer chains are entangled at the interface. The thickness of the primer layer is only about 1 μm, which minimizes the coated strut dimensions and the polymer load on the stent.

Stent retention processes for XIENCE V drug-coated stent were developed to assure that stent security, system profile, and stent deliverability are equivalent to the ML VISION stent, while preserving the integrity of the coating. Stent dislodgement testing showed that the XIENCE V DES has equivalent stent retention to the ML VISION stent. Engineering studies

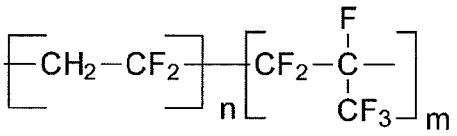

Figure 1. Chemical structure of PVDF-HFP.

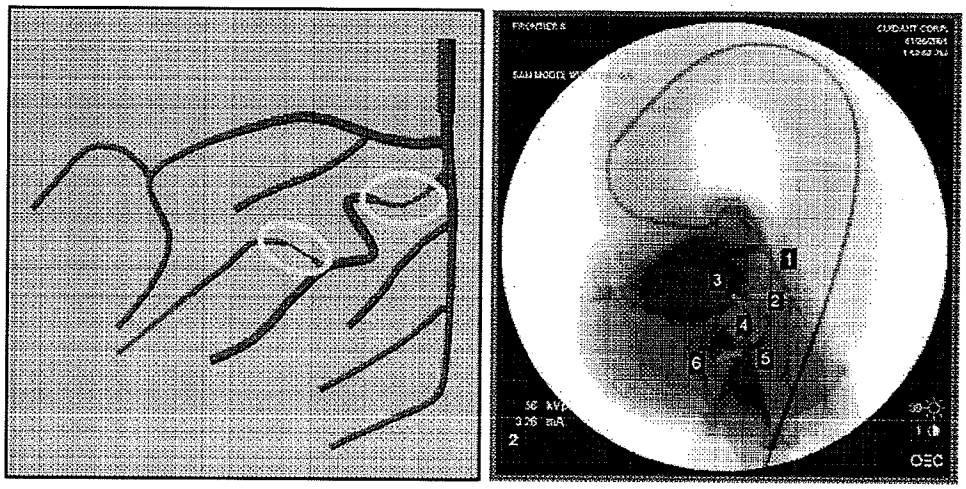

Figure 2. Design of synthetic vasculature model: Lumen of coronary artery (left panel) and an angiogram of the model (right panel). Numbers correspond to curves in track path of model.

have also demonstrated that the deliverability of the XIENCE V is equivalent to ML VISION in a synthetic vasculature model (Fig. 2). In this model, the stent delivery system was introduced by an experienced operator and advanced through the tortuosity until it could be advanced no further. A numerical score was assigned depending on how far the system progressed. Figure 3 summarizes data comparing XIENCE V with ML VISION. For all of the sizes tested in this model, the XIENCE V DES has demonstrated equivalent deliverability to ML VISION. XIENCE V also maintains a low system profile at 0.041″ (1.0 mm), which is comparable to the ML VISION stent profile of 0.040″ (1.0 mm) for 3.0 × 18 mm stent.

Hemocompatibility and Biocompatibility

Hemocompatibility (acute) and vascular biocompatibility (long-term) are of foremost importance in selecting a polymer as a drug-eluting reservoir. The characteristics determining the hemocompatibility and biocompatibility of an implanted biomaterial are many and complex and encompass more than just concepts

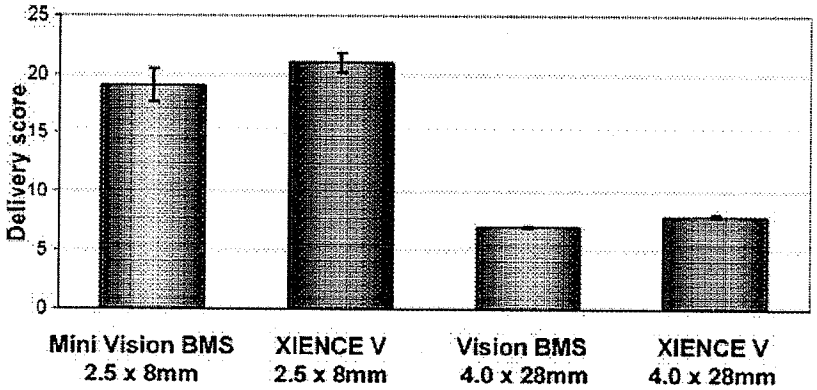

Figure 3. Illustration of synthetic test model and comparison data of XIENCE V DES deliverability with ML VISION bare metal stent (BMS) (n = 5). A higher score indicates better deliverability.

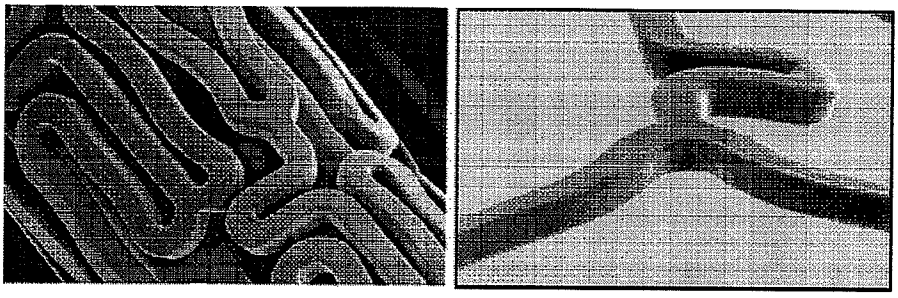

Figure 4. SEM images of the XIENCE V DES (scale = 150× in the left and 80× in the right).

of hydrophilicity and hydrophobicity. Factors such as surface chemistry, surface roughness, polymer purity, the presence of leachables and other impurities, in vivo stability of the polymer, and the interaction with blood-borne proteins all contribute to the blood and tissue compatibility of a polymer coating.

A critical first step in the interaction of a biomaterial with blood is the deposition of a protein-rich layer on the surface of the biomaterial. A high ratio of albumin to fibrinogen in this layer has been shown to greatly improve biocompatibility and hemocompatibility.[7–10] A series of studies[11–18] have shown that fluorine-rich surfaces are nonthrombogenic and biocompatibile. Such surfaces adsorb higher ratios of albumin to fibrinogen, resulting in significant reductions in platelet adhesion and activation.[11,12] Albumin adsorption passivates the fluorinated polymer surface, which contributes to thromboresistance, lack of complement activation, and the lower inflammation of fluorinated polymers in blood-contact applications in animal and in human.[13–16] Fluorination of polymer surfaces also increases the rate of reendothelialization of the vessel wall in animal models.[14] Due to their excellent hemocompatibility and biocompatibility, fluorinated polymers enjoy wide application in arterial prostheses, graft prostheses, drug-eluting leads of implantable cardioverter-defibrillators, hemodialysis membranes, vascular and neurovascular sutures, guidewire coatings, and in guiding catheters.[19] Preclinical studies performed at Abbott Vascular further confirm the hemocompatibility and biocompatibility of the XIENCE V PVDF-HFP polymer. These in vivo studies are discussed in a separate article in this supplement issue.

Polymer Properties. The PVDF-HFP polymer backbone is composed entirely of saturated carbon-carbon single bonds, which improves oxidative stability. These backbone carbon atoms are over 50%

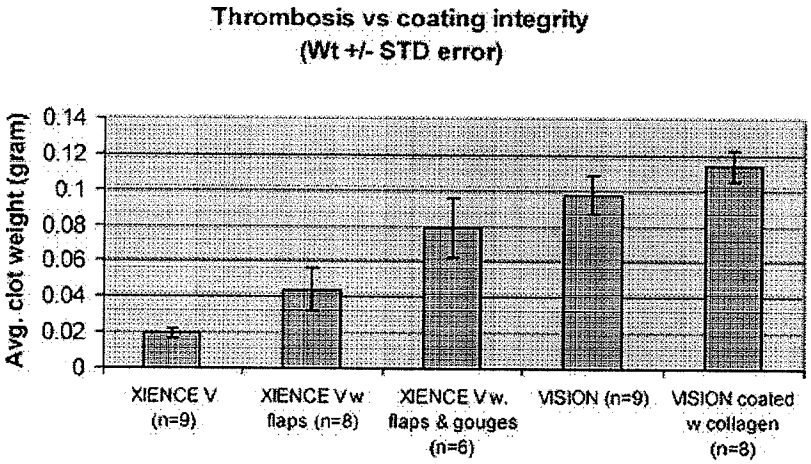

Figure 5. Relationship of thrombosis and coating integrity investigated in an ex vivo porcine femoral AV shunt model (3.0 × 18 mm stents).

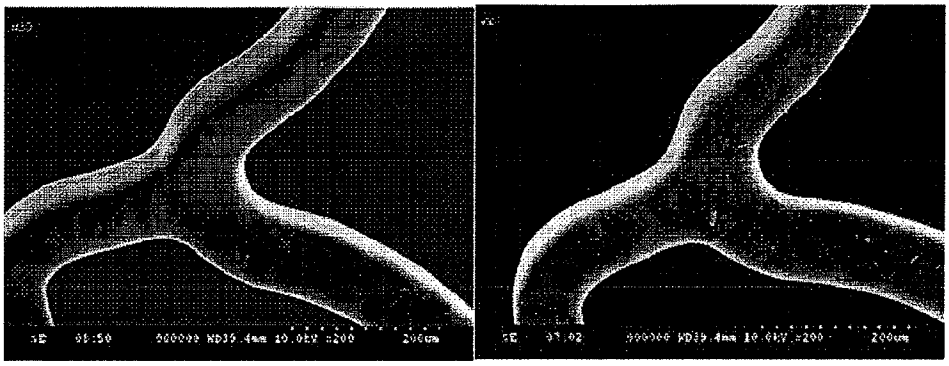

Figure 6. Representative SEM images of 10-year-accelerated fatigue test on overlapped XIENCE V DES with bending. The left image is prefatigue test and the right image is postfatigue test on nonoverlapped region. No change is observed.

fluorinated. The significance of fluorination is the high dissociation energy of the C-F bond that confers a high degree of chemical stability. Moreover, few carbon atoms with hydrogen substitution are adjacent to one another. This makes hydrogen radical abstraction to form carbon double bonds, a path to polymer degradation, unlikely. The absence of any reactive or enzymatically sensitive groups such as anhydride, ester, amide, ether, ketone, aldehyde, carbonate, or phosphate bonds makes the polymer resistant to hydrolytic, oxidative, or enzymatic cleavage. The lack of chemical reactivity of the polymer ensures no chemical interactions occur between PVDF-HFP and everolimus during the manufacturing process, on the shelf or in vivo. Similarly, this stable structure also ensures no chemical degradation takes place in vivo. Polymer chemical stability and the coating integrity were investigated in a swine model. In this study, everolimus-PVDF-HFP stents with a 200 $\mu g/cm^2$ drug dose were implanted for 3 months. After explantation, the polymer molecular weight was measured by gel permeation chromatography. For control stents stored at room temperature, the molecular weight was 287 K $\pm$ 2 K Daltons (n = 20), and for the explanted stents it was 284 K $\pm$ 13 K Daltons (n = 25). The difference was not statistically significant (P = 0.32), indicating the stability of the polymer in vivo.

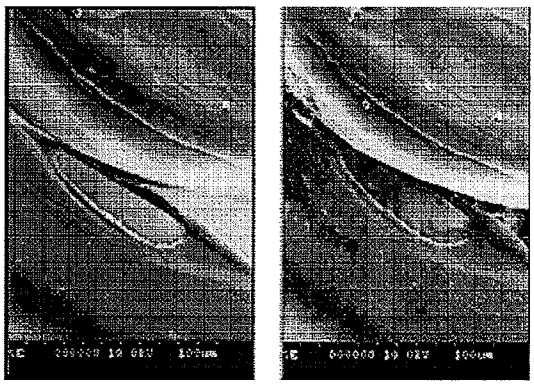

Figure 7. SEM images of 10-year-accelerated fatigue test on overlapped XIENCE V DES with bending. The left image shows the coating damage in the overlap region prefatigue test and the right images show the same damage region postfatigue test. No change is observed.

In this same study, the polymer mass was measured by ^{19}F nuclear magnetic resonance (NMR). After extracting the polymer off the stents, ^{19}F NMR spectroscopy allowed for selective quantification of the PVDF-HFP polymer. For controls stored at room temperature for 3 months, the mass recovery was 95.8 $\pm$ 3.0% (n = 5). For stents explanted after 3 months implantation, this recovery was 93.3 $\pm$ 2.3% (n = 5). The difference between the two groups was not statistically significant (P = 0.17), indicating the coating mass integrity was retained in vivo. These data demonstrate the stability of both molecular weight and mass for the coating and suggests that risk of inflammatory or other adverse biological responses caused by polymer degradation can be excluded.

For implantable materials, the purity of the polymer is essential for assuring a high level of biocompatibility. Total organic carbon extractable tests per United States Pharmacopeia (USP) on PVDF-HFP polymer have shown low levels of organic extractables at ppm levels. In addition, inductively coupled plasma mass

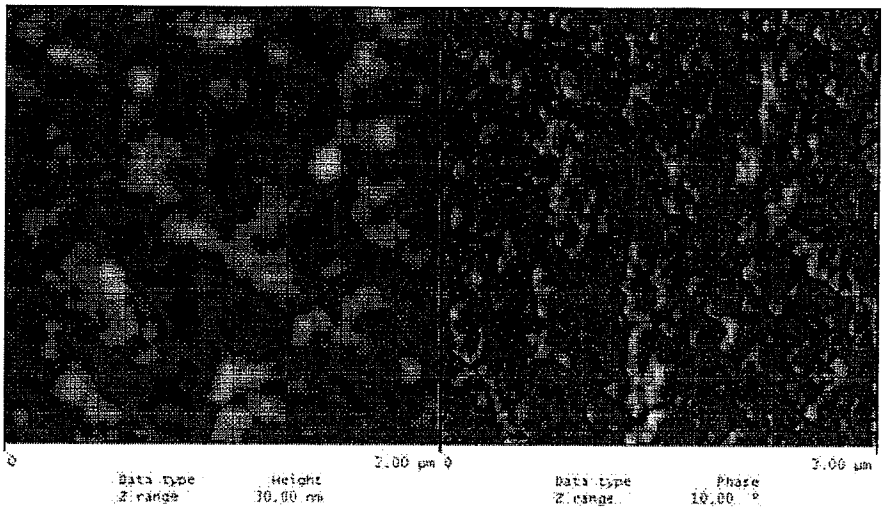

Figure 8. AFM topography image (left) and phase image (right) of XIENCE V coating on a 2 × 2 µm cross-section surface.

spectroscopy (ICP-MS) tests indicate that concentrations of heavy metals are at a sub-ppm level, thereby minimizing the risk of an inflammatory response or other adverse biological responses due to impurities.

Coating Integrity. For DES, the integrity of the coating is another important factor that can affect the hemocompatibility and biocompatibility of the system. It can also influence the uniformity of the drug delivery to the tissue. Suboptimal coating integrity may lead to coating particles being shed during delivery and expansion of the stents. Significant sections of missing coating expose the metal stent to the tissue and reduce the local drug delivery, thereby reducing the benefit of the drug. Coating particles and fragments released into the vessel wall may also elicit an inflammatory response at the site of implantation. Maintaining the integrity of the coating was a key design criterion for the XIENCE V DES. The selection of a semicrystalline, but flexible, fluorinated polymer, the design of the primer and drug reservoir construct, and the

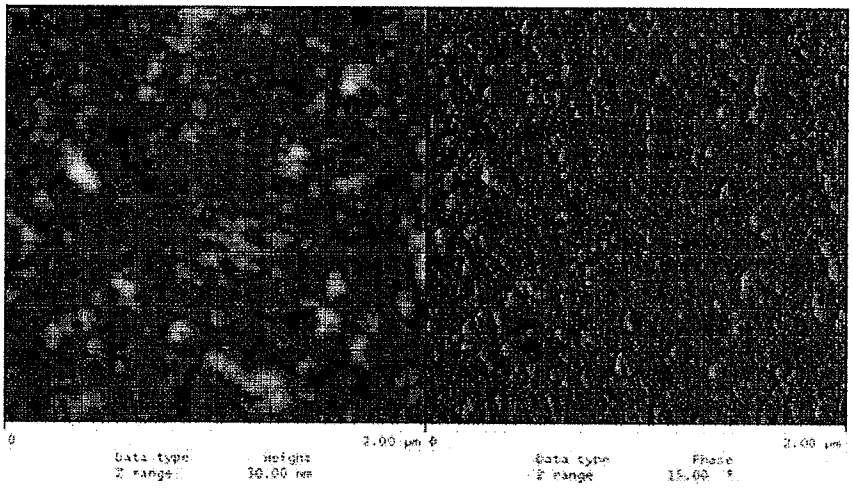

Figure 9. AFM topography image (left) and phase image (right) of polymer-only coating on a 2 × 2 µm cross-section surface.

Table 1. Thermal Properties of XIENCE V Coatings Relative to PVDF-HFP/PBMA Coatings with No Drug

ΔH_f % of Polymer-Only Stent (n = 6)	Melting Point % of Polymer-Only Stent (n = 6)
104 ± 8.6	99.0 ± 0.91

Table 2. Thermal Properties of XIENCE V Coatings after Aging at Ambient Conditions

Age	Drug Transition Temp., % of XIENCE V at T_0 (n = 6)	ΔH_f % of XIENCE V at T_0 (n = 6)
20 months	101 ± 1.9	98.6 ± 8.2
28 months	100 ± 1.8	92.4 ± 9.4

optimization of solvent-drug-polymer formulation resulted in exceptional coating integrity for the XIENCE V DES. Scanning electron microscope (SEM) analysis and bench testing confirm a smooth coating surface with minimal to no structural defects such as webbing, bridging, and strut-to-strut sticking (see Characterization section). Representative images of the XIENCE V coating as produced and after expansion are shown in Figure 4.

An acute ex vivo porcine femoral arteriovenous (AV) shunt model was employed to evaluate the influence of the coating defects on the hemocompatibility of XIENCE V stent. The model assessed thrombus formation and platelet deposition on XIENCE V stents as well as two groups of XIENCE V stents with intentionally modified coating surface. One group of XIENCE V stents were manufactured with luminal flaps and end ring defects. The second group had these same defects, but in addition, were intentionally scratched and the surface roughened with gauges. Controls were bare metal ML VISION and ML VISION coated with type I collagen. The XIENCE V DES exhibited minimal thrombus formation on the stent struts. Stents with more coating defects were more thrombogenic. ML VISION stents coated with hydrophilic collagen exhibited the highest thrombus formation. These study results demonstrated that the smooth and conformal fluorinated polymer coating surface on XIENCE V DES improves the thromboresistance (Fig. 5).

XIENCE V Coating Physical Characterization

Due to its glass transition temperature (T_g) of approximately –29 °C, the PVDF-HFP polymer is elastic with an ultimate elongation of over 600%. Such elasticity is essential for the coating to withstand stent deployment and postdilation without coating cracking or delaminating. PVDF-HFP is a partially crystalline polymer with a relatively low degree of crystallinity. Due to its low T_g and crystallinity, PVDF-HFP is tough and fatigue resistant. This allows the XIENCE V coating to withstand stent crimping forces and the abrasion/shearing forces encountered when delivering the stent to a challenging lesion with minimal coating damage. Engineering tests have demonstrated that the coating integrity is maintained after in vitro simulated delivery tests to the maximum labeled expansion of the stent, and after 10 years of accelerated radial fatigue testing (Figs. 6 and 7). In Figure 7, preexisting coating defects did not propagate after 10 years of

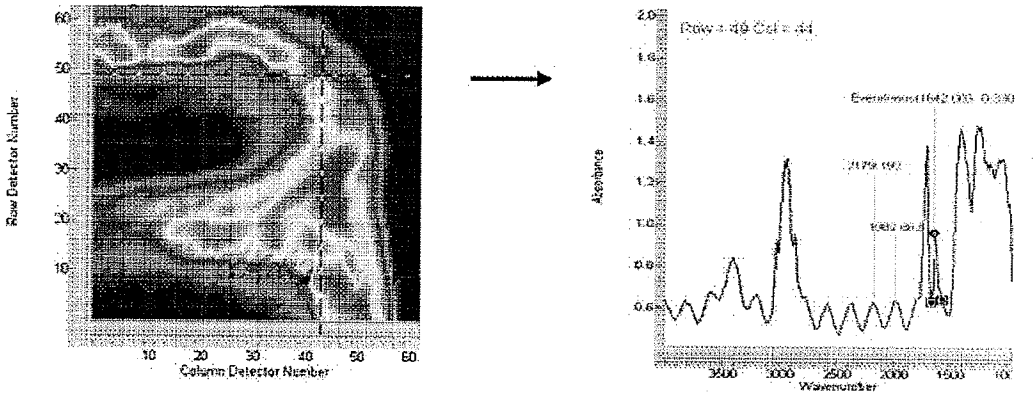

Figure 10. Representative FTIR drug distribution image on XIENCE V DES and FTIR spectrum showing interference pattern.

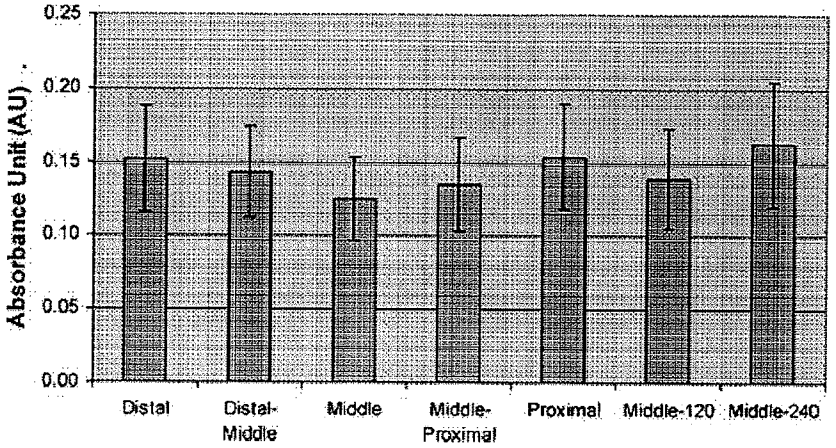

Figure 11. Drug distribution longitudinally (distal, distal-middle, middle, proximal, proximal-middle, and proximal) and circumferentially (120° and 240° rotation from middle) by imaging FTIR measurement (n = 30 spots per location).

accelerated fatigue testing. Chronic coating durability tests performed after tracking the preconditioned stents through tortuous paths, and deployment in synthetic arteries, show particulate counts comparable to that of the control blank synthetic artery, thereby indicating that the XIENCE V coating is durable.

Physical characterization studies indicate that the everolimus is uniformly dispersed in the polymer matrix at a nanometer scale as evidenced by atomic force microscopy (AFM) studies. Figure 8 shows a cross-section of the drug-polymer reservoir of a XIENCE V coating at a 2 × 2 μm scan size. At this magnification, the coating displays a high level of homogeneity over the entire cross-section. A fine, granular texture in the range of 70 nm is visible. A similar granular texture was also visible on cross-sectional analysis of a polymer-only stent (Fig. 9). The granular texture does not appear to be drug related and is believed to be due to the polymer. Consequently, no signs of phase separation between drug and polymer were detectable within the nanometer scale resolution of the method.

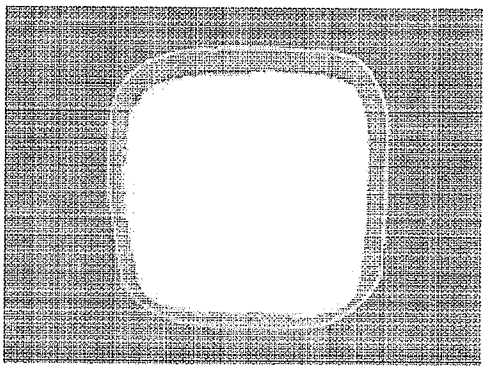

Figure 12. Representative cross-sectional SEM image of a XIENCE V stent strut with coating.

Thermal analysis was performed on XIENCE V stent coatings by differential scanning calorimetry (DSC). The thermograms show a melting endotherm due to the crystalline phase of the PVDF-HFP and a thermal transition due to the drug. A summary of these data and those from stent coatings with no drug is given in Table 1.

The presence of the drug in the polymer does not appreciably alter the PVDF-HFP degree of crystallinity or melting point. This indicates that coating properties that depend on polymer crystallinity, such as hardness and ultimate tensile strength, are less affected. Bulk everolimus exhibits a glass transition (T_g) at 87 °C. In the XIENCE V coating, the everolimus T_g is shifted down to 76 °C, with no transition evident at 87 °C. These data support the concept that no bulk everolimus is present in the coating. DSC analysis also shows that the melting enthalpy of the PVDF-HFP and the thermal transition temperature of everolimus do not change over time, indicating that the drug coating is at thermodynamic equilibrium after manufacture and sterilization (Table 2).

The distribution of the drug longitudinally and circumferentially in the XIENCE V coating was investigated by focal plane array imaging Fourier transform infrared spectroscopy (FTIR) in reflectance mode.

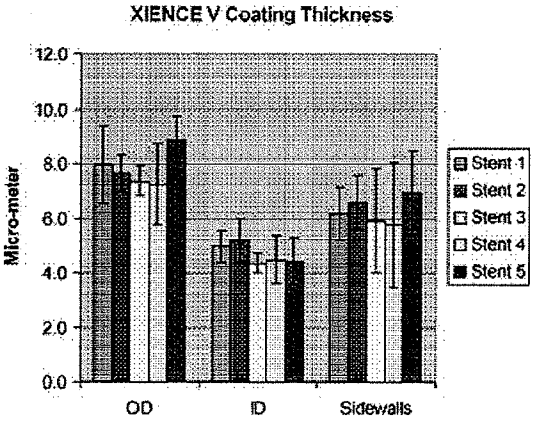

Figure 13. XIENCE V coating thickness data by cross-sectioning followed by SEM measurement. Fifteen struts per stent were sectioned for this analysis.

Figure 10 shows the XIENCE V drug distribution via this imaging technique where the spectra were gathered at an infrared wavelength specific to the drug. The relative drug concentration at each location is equivalent to the optical absorbance of this drug peak and can be used to quantify the relative drug distribution as a function of position. The color intensity corresponds to the total amount of drug integrated over the coating thickness at each point.

Three stents were used in this test. Seven stent positions covering the length and circumference were analyzed. At each location, absorption spectra for 10 randomly chosen points were obtained and averaged for the drug absorbance. Figure 11 shows the drug density (in infrared absorbance units) as a function of location on the stent. These results demonstrate a uniform drug distribution over the abluminal stent surface.

The coating thickness was measured by cross-sectioning the coated stent, followed by SEM analysis. The coated stents were first coated with a protective layer. The stent was then embedded in a resinous medium, sawed to make rough cross-sections and then polished. SEM images of each strut in cross-section were obtained (Fig. 12).

Care was taken to assure that the stent axis was orthogonal to the sectioning plane. The average coating thicknesses over the abluminal, luminal, and sidewall surfaces were measured with image analysis software (Fig. 13). The average coating thickness on the abluminal (OD) surface by this method was 7.8 ± 0.7 μm, and on the luminal surface (ID), 4.7 ± 0.4 μm.

Considering the drug characteristics in the polymer coating, the drug release mechanism is based primarily on the molecular diffusion of the drug through the polymer. This release mechanism results in a system with inherently high reproducibility for the drug release rate. The uniform drug distribution at both the micro- and macroscales also enables the tight control of the drug release rate across different manufacturing lines, from lot-to-lot and across multiple stent sizes to ensure precise delivery of the drug dose to patients (Fig. 14).

Conclusion

XIENCE V coating system is the result of research on multiple polymers, combined with extensive coating

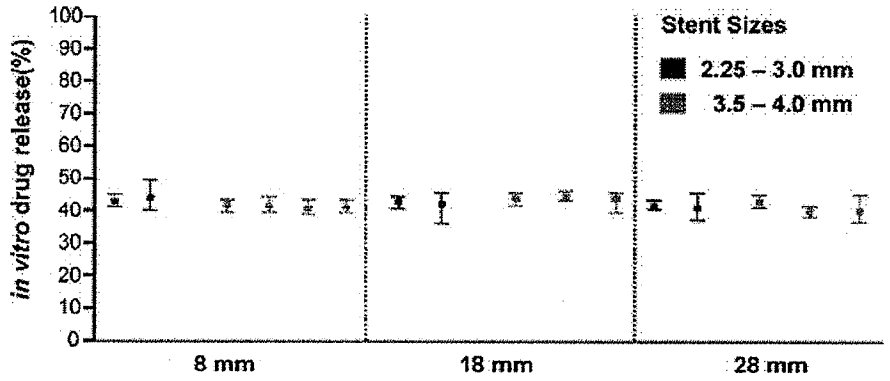

Figure 14. In vitro percent drug release of Xience V DES demonstrates consistent drug release rate on different stent sizes, lot-to-lot, and within the lot. Stents from the same lot were coated on different coating equipment.

formulation and design iteration. A fluorinated copolymer drug reservoir coating was chosen based on the history of use of fluorinated polymers in a blood-contacting environment, the ability to control the drug release, and mechanical properties amenable to stent expansion and use. Bench characterization and preclinical evaluation results, as discussed in a separate article in this supplement issue, demonstrate that XIENCE V is highly deliverable, and the coating is biocompatible and possesses exceptional coating integrity. Clinical data from the SPIRIT series of human clinical trials[1,2,20] support the safety and effectiveness of the XIENCE V, a second-generation DES.

Acknowledgments: The authors would like to express their sincere gratitude to Murthy Simhambhatla, Krishna Sudhir, Wai-Fung Cheong, Andrew Tochterman, and Sue Silavin for reviewing the article, to Syed Hossainy for providing valuable references, to Shawn Chin-Quee and George Abraham for providing ex vivo study results, and to David Wolf-Bloom for providing the stent deliverability data and reviewing the article. Last, we wish to thank the many members of the XIENCE V team whose dedication and sacrifice made the XIENCE V product a reality.

References

1. Ruygrok P, Desaga M, Van Den Branden F, et al. One year clinical follow-up on the XIENCE V Everolimus-eluting stent system in the treatment of de novo native coronary artery lesions: The SPIRIT II study. EuroIntervention 2007;3:315–320.
2. Stone GW, Midei M, Newman W, et al. Comparison of an everolimus-eluting stent and a paclitaxel-eluting stent in patients with coronary artery disease: A randomized trial. JAMA 2008;299:1952–1953.
3. Joner M, Nakazawa G, Finn AV, et al. Endothelial cell recovery between comparator polymer-based drug-eluting stents. J Am Coll Cardiol 2008; 52:333–342.
4. Schuler W, Sedrani R, Cotton S, et al. SDZ RAD, a new rapamycin derivative. Transplantation 1997;64:36–42.
5. Adamson, A. Physical Chemistry of Surfaces, 4th ed. New York: John Wiley, 1982, p352, p413.
6. Available at: http://www.fda.gov/ohrms/dockets/dailys/04/sep04/091704/03m-0172-sup00001-vol1.pdf
7. Eberhart RC, Clagett CP. Catheter coatings, blood flow, and biocompatibility. Semin Hematol 1991;28(4 suppl 7):42–48; discussion 66–68.
8. Mulvihill JN, Faradji A, Oberling F, et al. Surface passivation by human albumin of plasmaperesis circuits reduces platelet accumulation and thrombus formation. Experimental and clinical studies. J Biomed Mater Res 2004;24:155–163.
9. Park K, Kamath KR. Surface modification of polymeric biomaterials by albumin grafting using γ-irradiation. J Appl Biomater 2004;5:163–173.
10. Kottke-Marchant K, Anderson JM, Umemura Y, et al. Effect of albumin coating on the in vitro blood compatibility of Dacron® arterial prostheses. Biomaterials 1989;10:147–155.
11. Hasebe T, Yohena S, Kamijo A, et al. Fluorine doping into diamond-like carbon coatings inhibits protein adsorption and platelet activation. J Biomed Mater Res 2007;83A:1192–1199.
12. Hasebe T, Ishimaru T, Kamijo A, et al. Effects of surface roughness on anti-thrombogenicity of diamond-like carbon films. Diamond & Related Mater 2007;16(N4–7):1343–1348.
13. Pedrini L, Dondi M, Magagnoli A, et al. Evaluation of thrombogenicity of fluoropassivated polyester patches following carotid endarterectomy. Ann Vasc Surg 2001;15:679–683.
14. Guidoin R, Marois Y, Zhang Z, et al. The benefits of fluoropassivation of polyester arterial prostheses as observed in a canine model. ASAIO J 1994;40:M870–M879.
15. Chinn JA, Sauter JA, Phillips RE, Jr, et al. Blood and tissue compatibility of modified polyester: thrombosis, inflammation, and healing. J Biomed Mater Res 1998;39:130–140.
16. Hasebe T, Shimada A, Suzuki T, et al. Fluorinated diamond-like carbon as antithrombogenic coating for blood-contacting devices. 2006;76a:86–94.
17. Petersen RJ , Rozelle LT. Ethylcellulose perfluorobutyrate: A highly non-thrombogenic fluoropolymer for gas exchange membranes. Trans Am Soc Artif Intern Organs 1975;21:242–248.
18. Liu TY, Lin WC, Huang LY, et al. Surface characteristics and hemocompatibility of PAN/PVDF blend membranes. Polym Adv Technol 2005;16:413–419.
19. Karl Graffte. Fluoropolymers: Fitting the bill for medical applications. MDDI 2005;Oct:34–37.
20. Beijk, MA, Neumann FJ, Weimer M, et al. Two-year results of a durable polymer everolimus-eluting stent in de novo coronary narrowing (The SPIRIT FIRST Trial). EuroIntervention 2007;1:266–272.